Sensitivity Analysis of Near-Wall Turbulence Modeling for Large Eddy Simulation of Incompressible Flows

KHAN RAQIB MAHMUD

Master of Science Thesis
Stockholm, Sweden 2014

Sensitivity Analysis of Near-Wall Turbulence Modeling for Large Eddy Simulation of Incompressible Flows

K H A N R A Q I B M A H M U D

Master's Thesis in Scientific Computing (30 ECTS credits)
Master Programme in Computer simulation for Science and Engineering (120 credits)
Royal Institute of Technology year 2014
Supervisors at KTH were Johan Hoffman and Aurélien Larcher
Examiner was Michael Hanke

TRITA-MAT-E 2014:33
ISRN-KTH/MAT/E--14/33--SE

Royal Institute of Technology
School of Engineering Sciences

KTH SCI
SE-100 44 Stockholm, Sweden

URL: www.kth.se/sci

Abstract

Wall layer models are very important for the simulation of turbulent flows in complex geometries to characterize the significant flow features. For the simulation of turbulent flows, the performance of Large Eddy Simulation techniques with different wall layer models which we refer to as near-wall turbulence modeling for turbulent flows are analyzed. The wall shear stress model and Delayed Detached Eddy Simulation wall model are two options, that can be used to model the turbulent boundary layer. In this project, a wall shear stress model is used as a near-wall turbulence model in the G2 simulation technique. A sensitivity analysis of this near-wall turbulence modeling with respect to model parameters in the simulation techniques of incompressible turbulent flows is presented.

Sammanfattning

Känslighetsanalys av modellering av väggnära turbulens för Large Eddy Simulering av inkompressibla flöden

Väggmodellering är viktigt i simuleringar av turbulenta flöden i komplexa geometrier då de mest inverkande flödesegenskaperna ska karakteriseras. Prestandan hos Large Eddy Simulation-tekniker med olika väggmodeller analyseras för simuleringar av turbulenta flöden med höga Reynoldstal. Två alternativ som kan användas för turbulenta gränsskikt är "Wall Shear Stress Model" och "Delayed Detached Eddy Simulation Wall Model". I detta projekt används en wall shear stress modell för det turbulenta flödet vid väggen tillsammans med G2 simuleringsmetodiken. En känslighetsanalys av denna modell med hänsyn till modellparameterar presenteras för simuleringar av inkompressibla turbulenta flöden.

Acknowledgements

First, all the praises and thanks be to Almighty Allah who has given me the energy and ability to complete my thesis project successfully.

I would like to express my sincere gratitude and profound respect to my thesis supervisor Professor Dr. Johan Hoffman, Department of High Performance Computing and Visualization, for giving me the opportunity to work on this thesis project in his wonderful CTL (Computational Technology Laboratory) group.

Dr. Aurélien Larcher, technical supervisor of my thesis work, postdoc researcher, Department of High Performance Computing and Visualization, without whom it would have been impossible to write this thesis, my heartiest thanks to him for showing me the ways of thinking new ideas for a research work, for discussing about the physical phenomena and numerical solutions and complexity, and for his invaluable suggestions, help and support in every stage of my thesis work.

I would like to convey my deepest thanks and respect to the program coordinator of the Erasmus Mundus masters programme COSSE associate Professor Dr. Michael Hanke, department of Numerical Analysis, for his continuous support and guidance in all cases of my study at KTH, Sweden.

Finally, My deepest thanks and love to my parents and my dearest younger brother for their encouragement, support, love and blessings.

Contents

List of Figures

List of Tables

Chapter 1

Introduction

Computational modeling of high Reynolds number turbulent flows is still a great challenge that faces a number of open problems in mathematics, numerical analysis and fluid dynamics. For the simulation of turbulent flows, Large Eddy Simulation (LES) is one of the adequate techniques when dynamic features of the turbulent flows are needed.

The thesis is mainly concerned with the investigation and development of near-wall turbulence modeling for LES of incompressible flows. The past decade has seen a promising development of the mathematical theory of LES of incompressible flows and in particular the investigation of Implicit LES models. In the frame of the General Galerkin method (G2) the effect of unresolved scales is taken into account by an implicit subgrid model built from numerical stabilization of the finite element scheme. The performance of the class of LES models is intrinsically limited by the numerical treatment of boundary walls and this remains a challenge due to the prohibitive computational cost as integrating the solution in the boundary layers requires mesh refinement and from a physical point of view as complex wall bounded flows can be highly sensitive to the friction enforced.

In this project we investigate the sensitivity of wall modeling with respect to model parameters in LES of incompressible turbulent flows in different geometries.

A first option to model the turbulent bounday layers is the wall shear stress model where the tangential velocity is prescribed with the shear stress model and a skin friction parameter chosen based on the Reynolds number and the roughness of the boundary.

The accuracy and efficiency of Large Eddy Simulation with near-wall turbulence modeling for complex turbulent flows are investigated in the project by considering two different test cases and the motivation to consider the test cases is that similar types of real engineering problems are very common. We find that the wall model captures correctly the delayed separation and computed correctly the reattachment length for flows in a complex geometry.

The sensitivity of the skin friction parameter of wall shear stress modeling on the flow field is studied and the results are analyzed according to the physics of the flow. Wall shear stress models that provide no slip, pure slip and slip

with friction boundary conditions by parameter changing are employed with the LES.

Numerical studies on two dimensional channel flows across a step and flow past a circular cylinder in two dimension using these wall modeling are presented. An experimental validation is performed by comparing the numerical results with the experimental results that are published into the journals to validate the wall shear stress model. Finally, the results are analyzed and the observations for the sensitivity of the near-wall modeling employed with the LES are presented.

Chapter 2

Large Eddy Simulation Techniques

Many fluid flows that occur in nature as well as in engineering applications are turbulent flows. Turbulent flows have complex and chaotic variation in space and time on a wide range of scales from small to large, so it is very difficult to give an accurate definition of turbulence and normally these flows appear for fluids with small viscosity, such as air and water.

There are certain flow features that can be observed in turbulent flows described in [18, p. 1-3]: Unpredictability which is defined as the irregularity of the flow downstream separation that makes a deterministic description of the motion impossible as a function of time and space coordinates. Shear layer that originates from the separation line is a region of strong coherent vorticity therefore in the analysis of turbulent flows vorticity fluctuations have important role. Diffusivity is one of the most significant features of turbulent flows and if the distance from separation increases the diffusion of velocity fluctuations becomes stronger.

There are numerous approaches to the simulation of turbulent flows available and LES is one promising approach for turbulence simulation which is studied with near wall modeling in this project.

2.1 Introduction

The LES technique computes the large eddies of a turbulent flow accurately above a preassigned length scale and the effect of the small scale flow structures onto the large scale flows is modeled.

For the LES technique in which approximations to the local spatial averages of the fluid's velocity are computed, the LES equations are solved over moderate time intervals and special care needs to be taken to find the appropriate boundary conditions for the flow averages which depend on the behavior of the unknown flow near the wall.

LES is performed in the physical space in most cases with the use of some numerical schemes that introduce an additional dissipation. As a result, the

scheme acts as a numerical filter that damps the highest resolved frequencies of the flow. So the filtering operation is widely assumed to be implicit due to a combination of the mesh and the intrinsic dissipation of the numerical scheme.

A new approach to computational turbulence modeling was introduced in [10] which is referred to as General Galerkin (G2) turbulence simulation, described in section 2.6. In the frame of G2 turbulence simulation, turbulence is modeled by weak solutions to the Navier–Stokes equations and a stabilized finite element method is used to compute approximations with *a posteriori* error control based on the error in the functional output.

In this project, we have studied the effect of a near-wall turbulence model that has been used with this G2 turbulence simulation technique.

A Spalart–Allmaras simulation technique is studied which is implemented in a style of Delayed Detached Eddy Simulation model which is a near wall model for the turbulent simulation.

2.2 Analysis of Numerical Errors and Reliability of LES

Error estimation in Reynolds averaged Navier–Stokes (RANS) simulation and LES is of great interest today where RANS simulation is a different technique in which RANS equations are formulated by taking time averaging the standard Navier–Stokes equations. The main challenge for LES is not lying anymore in the development of new modeling or regularization approaches. Apart from that unresolved problem of LES and high Reynolds number boundary layers, most of the techniques produce very satisfactory results when used appropriately. A fully consistent theory on errors in LES still requires a huge amount of work. LES involves three essential features:

1. assessment of modeling errors committed in approximating
2. assessment of numerical errors in solving the resulting system and
3. correct boundary conditions for flow averages

Boundary conditions must be supplied for the large eddies as they do not adhere to solid walls. So the large eddies should satisfy a no-penetration condition and a slip with friction condition on boundary.

In the frame of the G2 method, the effect of unresolved scales is taken into account by an implicit subgrid model built from numerical stabilization of the finite element scheme [11]. The stabilization of the Galerkin method giving a streamline diffusion stability of the finite element space discretization scheme acts as the subgrid model in the LES. The *a posteriori* error estimate takes into account both the error from discretization and the error from the subgrid model. The important observation is that, the contribution from subgrid modeling in the *a posteriori* error estimation is small, making it possible to simulate aspects of turbulent flow without accurate modeling of Reynolds stresses.

2.3 Computational Model

The incompressible Navier–Stokes equations are part of many complex models in science and engineering applications. The laminar or turbulent flow of an incompressible fluid is modeled by the solutions of the incompressible Navier–Stokes equations.

2.3.1 Incompressible Homogeneous Navier–Stokes Equations

We consider the incompressible homogeneous Navier–Stokes equations as the basic model in which incompressibility expresses that the density ρ is a function of pressure p, $\rho = \rho(p)$ and does not change with pressure i.e. the Lagrangian derivative of ρ is equal to zero, $\frac{D\rho}{Dt} = 0$. The homogeneity implies that the density is constant everywhere i.e. $\rho(., t) =$ constant. The equations express conservation of momentum and conservation of mass or the continuity equation with incompressibility and isothermal i.e. constant temperature for a Newtonian fluid with viscous stresses depending linearly on velocity gradients and constant kinematic viscosity $\nu > 0$ enclosed in a volume $\Omega \subset \mathbb{R}^3$ over a time interval $I = (0, T]$, where Ω is a polygonal:

$$\begin{aligned} \dot{u} + (u \cdot \nabla)u - \nu\Delta u + \nabla p &= f, && (x,t) \in \Omega \times I \\ \nabla \cdot u &= 0, && (x,t) \in \Omega \times I \\ u(x,0) &= u^0(x), && x \in \Omega \end{aligned} \tag{2.1}$$

where $u(x,t)$ is the velocity vector, $p(x,t)$ is the pressure, $u^0(x)$ is the initial data and $f(x,t)$ is the body force.

The quantity $\nu\Delta u - \nabla p$ represents the total fluid force and can be expressed as

$$\nu\Delta u - \nabla p = \mathrm{div}\sigma(\mathrm{u}, \mathrm{p})$$

where $\sigma(u,p) = (\sigma_{ij}(u,p))$ is the Cauchy stress tensor.

The stress tensor $\sigma_{ij} = 2\nu\epsilon_{ij}(u) - p\delta_{ij}$ with strain rate tensor $\epsilon_{ij}(u) = 1/2(\partial u_i/\partial x_j + \partial u_j/\partial x_i)$ and δ_{ij} the Kronecker delta function, and the relative importance of viscous and inertial effects in the flow determined by the Reynolds number $Re = UL/\nu$, where U and L are characteristic velocity and length scales.

If we assume that equation (2.1) is non-dimensionalized by the reference velocity U and typical length scale L so that U and L are both equal to one, we get the Reynolds number Re is equal to ν^{-1}.

2.3.2 Mathematical Analysis of Navier–Stokes Equations

The mathematical theory of Navier–Stokes equations for small ν does not give assurance the existence of classical solutions.

Using methods from functional analysis, the existence of an exact weak solution to the Navier–Stokes equations was proved by Jean Leray in 1934 where the residual tested a suitable set of smooth test functions. But the uniqueness

and regularity of Leray's weak solutions of Navier–Stokes equations has not yet been proven in 3D.

Well-posedness means that small variations in data result in small variations in the solution which can be relaxed as a question of output sensitivity of perturbations. Weak uniqueness (uniqueness in output) of the Navier–Stokes equations has been proved by where an approximate weak solutions is constructed using a G2 method by solving an associated dual problem computationally, with data coupling to the particular output [10].

2.4 Boundary Conditions

The computational domain Ω is often artificially truncated so that inflow and outflow boundary conditions need to be specified. An inflow boundary Γ_{inflow} is typically modeled as a Dirichlet boundary condition for the velocity, using a finite element method, implemented in the weak form.

A Neumann boundary condition $\sigma \cdot n = g$ can be used with $g = 0$ to model an outflow boundary corresponding to zero stress at the outflow as in outflow into a large empty reservoir. If the viscous term appear variationally, the corresponding Neumann boundary condition acts as an approximate transparent outflow boundary condition, attempting to let the flow leave the domain with little obstruction also referred as a "do nothing" boundary condition.

At a solid boundary Γ_{solid} a no slip boundary condition can be applied, enforcing the velocity of the solid boundary as a homogeneous Dirichlet boundary condition for the fluid $u = 0$, and a free slip boundary condition can be applied as a normal component of the velocity is set to zero, $u \cdot n = 0$. A slip with friction boundary condition corresponds to setting the normal component of the velocity to zero at the solid boundary together with a friction condition on the tangential velocity. Such boundary conditions are more suitable for LES where large eddies of a turbulent flow are computed accurately, to describe the phenomena such as main vortices, move on the boundary (slip) and loose energy while moving (friction).

A turbulent boundary layer is impossible to resolve as the Reynolds number increases in practical applications so the turbulent boundary layer must be modeled, two different options for wall layer models to model the turbulent boundary layer are discussed in chapter 3.

2.5 Numerical Methods

2.5.1 Weak Formulation

We define a pair of test functions $\hat{v} = (v, q) \in \widehat{V}$ where $\widehat{V}$ is a test function space defined by,

$$\widehat{V} = \{\hat{v} \in H^1(Q)^4 : v \in L_2(I; H_0^1(\Omega)^3)\}$$

over the space-time domain $Q = \Omega \times I$ where

$$L_2(I;\Omega) := \left\{ v : I \mapsto \Omega \,\middle|\, \int_\Omega v^2 < \infty \right\}$$

denotes the space of square-integrable Lebesgue functions. We choose $((.,.))$ is the $L_2(Q)^m$ inner product with $m = 1, 3$ or a suitable duality pairing over the space-time domain Q.

The space

$$H^1(\Omega) := \left\{ v : \Omega \mapsto R \,\middle|\, v, \nabla v \in L_2(\Omega) \right\}$$

denotes the corresponding Sobolev space of functions that have square-integrable derivatives and $H_0^1(\Omega)$ is the Sobolev space of functions being zero on the boundary Γ and square-integrable together with their first derivatives over $\Omega \subset \mathbb{R}^3, \Omega \neq \varnothing$ with boundary $\Gamma = \partial\Omega$, with dual $H^{-1}(\Omega)$.

Then the weak formulation of equation (2.1) can be obtained by multiplying (2.1) with the pair of test functions $\hat{v} = (v, q) \in \hat{V}$ and integrating over the domain Ω. So the weak problem is to find $\hat{u} = (u, p)$ such that

$$\int_Q \dot{u} \cdot v + \int_Q (u \cdot \nabla u).v + \int_Q \sigma : \nabla v - \int_{\Gamma \times I} \sigma v \cdot n ds - \int_Q f.v = 0$$
$$\int_Q \nabla \cdot u \cdot q = 0$$

Here ":" denotes double dot product which is sum of the products over all components and all derivatives *i.e.* $\sigma : \nabla v = \sum_{i=1}^{i=3} \sum_{j=1}^{j=3} (\sigma)_{ij} (\nabla v)_{ij}$, $\int_Q u \cdot v$ denotes $\int_I \int_\Omega u \cdot v dx dt$, $\sigma(u, p) = \sigma_{ij} = 2\nu\epsilon_{ij}(u) - p\delta_{ij}$ and the part $\int_{\Gamma \times I} \sigma v \cdot n ds = \int_{\Gamma \times I} (2\nu\epsilon(u) - p\delta_{ij}) v \cdot n ds = 0$ as we impose Neumann boundary conditions on one part of the boundary and $u = 0$ on the remaining part. So the weak form becomes,

$$\int_Q \dot{u} \cdot v + \int_Q (u \cdot \nabla u).v + \int_Q \sigma : \nabla v - \int_Q f.v = 0$$
$$\int_Q \nabla \cdot u \cdot q = 0$$

We write this weak problem into the short form,

$$\begin{aligned} ((R(\hat{u}), \hat{v})) \equiv ((\dot{u}, v)) + (((u \cdot \nabla)u, v)) - ((\nabla \cdot v, p)) + ((\nabla \cdot u, q)) \\ + ((2\nu\epsilon(u), \epsilon(v))) - ((f, v)) = 0 \end{aligned} \tag{2.2}$$

where $((u, v)) = \int_I \int_\Omega u \cdot v dx dt$.

2.5.2 Time Discretization Scheme

A classical time-discretization scheme known as the θ-scheme can be defined as,

$$\frac{u^{n+1} - u^n}{\delta t} + \theta F(u^{n+1}) + (1 - \theta) F(u^n) = f, \qquad \theta \in [0, 1] \tag{2.3}$$

for a scalar and linear problem:

$$\frac{\partial u}{\partial t} + F(u) = f$$

For $\theta = \frac{1}{2}$, the method (2.3) is an implicit method known as Crank–Nicolson method.

The Crank–Nicolson method has an accuracy of order $O(\Delta t^2)$. Also for a convection dominated problem this method is unconditionally stable and does not have damping property.

Now for the time discretization of the weak formulation (2.2) of the Navier–Stokes equations (2.1), we use Crank–Nicolson method.

Let $0 = t_0 < t_1 < t_2 < \ldots < t_N = T$ be a sequence of discrete time steps with associated time intervals $I_n = (t_{n-1}, t_n)$ of length $k_n = t_n - t_{n-1}$, then the time discretization of the weak problem (2.2) is the following:

$$\begin{aligned}&((u^n - u^{n-1})k_n^{-1} + \hat{u}^n \cdot \nabla \hat{u}^n, v) + (2\nu\epsilon(\hat{u}^n), \epsilon(v)) - (p^n, \nabla \cdot v) + (\nabla \cdot \hat{u}^n, q)\\ &= (f, v)\end{aligned} \tag{2.4}$$

where $\hat{u}^n = \frac{1}{2}(u^n + u^{n-1})$. This approach requires to solve a nonlinear problem at each time step.

2.5.3 Space Discretization: Finite Element Method

For finite element space discretization of the weak form (2.4) of Navier–Stokes equations, we choose Lagrange P1/P1 elements (continuous linear velocity and pressure) which is equal order interpolation velocity–pressure elements.

We seek $\widehat{U} = (U, P)$, continuous piecewise linear in space and time, and the space discretization for NSE (2.1) with homogeneous Dirichlet boundary conditions reads: for $n = 1, \ldots, N$ find $(U^n, P^n) \equiv (U(t_n), P(t_n))$ with $U^n \in V_0^n \equiv [W_0^n]^3$ and $P^n \in W^n$ where $W^n \subset H^1(\Omega)$, such that

$$\begin{aligned}&((U^n - U^{n-1})k_n^{-1} + \widehat{U}^n \cdot \nabla \widehat{U}^n, v) + (2\nu\epsilon(\widehat{U}^n), \epsilon(v)) - (P^n, \nabla \cdot v) + (\nabla \cdot \widehat{U}^n, q)\\ &= (f, v) \qquad \forall \hat{v} = (v, q) \in V_0^n \times W^n\end{aligned} \tag{2.5}$$

Concerning the stability of the space discretization we see that this discretization is not stable since it does not satisfy the inf–sup stability condition. The stable and convergent choices for the finite element spaces are those which satisfy the following inf–sup or Babuska–Brezzi condition [6, p.81], [22, 2]:

$$\inf_{0 \neq P^n \in W^n} \sup_{0 \neq U^n \in V^n} \frac{(P^n, \nabla \cdot U^n)_\Omega}{\|P^n\|_{L_0^2(\Omega)} \|U^n\|_{H^1(\Omega)}} \Bigg\} \geq \gamma > 0 \tag{2.6}$$

where γ is a constant independent of mesh size.

So as the P1/P1 discretization is not compatible with the inf–sup condition, we can add certain stabilizing term to control spurious pressure oscillations to resolve the stability problem.

2.5.4 Stability and Consistency of Discretization Schemes

For high Reynolds number flow problems, the finite element discretization may become unstable since they use central differences for discretizations of the advective term. To avoid this instability problem some numerical damping is required. Weighted Least squares approaches can be used which add certain least square terms to the discretization gives the stability.

Firstly, to avoid the problem of instability, we use a method in the context of finite element discretization that adds artificial viscosity using the Streamline Diffusion method, discussed in 2.6. The idea of Streamline diffusion is to produce artificial diffusion acting only in the transport direction while maintaining the second order consistency of the scheme [3]. This can be done by adding certain least square terms to the discretization.

Secondly, We can add some artificial viscosity physically by using the Spalart–Allmaras model, discussed in 2.7.

We discussed these two stability approaches into the following sections as two different kind of simulation techniques that we used into the project.

Time Stepping for Stability

Time stepping is important for the numerical stability and to resolve the turbulent motions accurately in time. For the stability, the choice of time stepping used into the LES approach, one of the following conditions can be applied [30, p.557]:

The viscous condition is:

$$\Delta t < \Delta t_v = \sigma \frac{\Delta y^2}{\nu} \tag{2.7}$$

where Δy is the cell size in the y direction and σ depends on the actual time stepping.

The CFL condition which is applied in our simulation method, for the time step Δt is:

$$\Delta t < \Delta t_c = \mathrm{CFL} \frac{\Delta x}{U_c} \tag{2.8}$$

where Δx is the cell size in the x direction, U_c is a convective velocity and CFL is the maximum allowable courant number that depends on the numerical scheme used.

2.5.5 Linearization and Linear Solver

The finite element discretization of the Navier–Stokes equation (2.1) consists of a nonlinear term into the stiffness matrix so a system of nonlinear equations have to be solved. To solve this system of nonlinear equations an iterative procedure is necessary.

An iterative procedure works in a way:

1. First make an initial estimation

2. Then linearize the nonlinear equations based on the previous solution

3. Finally solve the resulting system of linear equations

4. If the solution does not converge, go to step 2; otherwise stop

We use such a method to solve the system of nonlinear equations: Picard fixed point iteration method. As for the time discretization we use Crank–Nicolson scheme, it requires in each time step linearize the system of nonlinear equations and solve the system of linear equations.

For solving the system of linear equations we use Krylov iterative solver in our simulation software.

2.6 General Galerkin (G2) Simulation Technique

2.6.1 Streamline Diffusion Stability

We add certain least square terms to the finite element discretization (2.5) for the streamline-diffusion stability *i.e.* add a diffusion term acting only in the direction of the streamlines that gives a good stability and high accuracy [7, 4],then the discretization is [10, p.212]:

$$\begin{aligned}&((U^n - U^{n-1})k_n^{-1} + \widehat{U}^n \cdot \nabla \widehat{U}^n, v) + (2\nu\epsilon(\widehat{U}^n), \epsilon(v)) - (P^n, \nabla \cdot v) + (\nabla \cdot \widehat{U}^n, q)\\ &+ SD_\delta^n(\widehat{U}^n, P^n; v, q) = (f, v) \qquad\qquad \forall \hat{v} = (v, q) \in V_0^n \times W^n\end{aligned} \tag{2.9}$$

where $\widehat{U}^n = \frac{1}{2}(U^n + U^{n-1})$ and P^n are piecewise constant in time over I_n with the stabilizing term

$$\begin{aligned}SD_\delta^n(\widehat{U}^n, P^n; v, q) \equiv (\delta_1(\widehat{U}^n \cdot \nabla \widehat{U}^n + \nabla P^n - f), \widehat{U}^n \cdot \nabla v + \nabla q)\\ + (\delta_2 \nabla \cdot \widehat{U}^n, \nabla \cdot v)\end{aligned} \tag{2.10}$$

and

$$(v, w) = \sum_{K \in \mathcal{T}} \int_K v \cdot w dx$$

with the stabilization parameters

$$\begin{aligned}\delta_1 &= K_1(k_n^{-2} + |U^{n-1}|^2 h_n^{-2})^{-1/2}\\ \delta_2 &= K_2 h_n\end{aligned} \tag{2.11}$$

where K_1 and K_2 are positives constants of unit order.

For turbulent flow the size of the time step is chosen as:

$$k_n \sim min_{x \in \Omega}(h_n / |U^{n-1}|) \tag{2.12}$$

so that

$$\delta_1 \sim k_n \sim min_{x \in \Omega}(h_n / |U^{n-1}|)$$

2.7 Spalart–Allmaras Simulation Technique

2.7.1 Stability by adding viscosity from DDES model

For the second approach of stabilizing the finite element discretization (2.5), we add an artificial viscosity which comes from a physical model Delayed Detached Eddy Simulation (DDES) model.

We add viscosity form DDES based on the Spalart–Allmaras (SA) model, so we referred this simulation technique as Spalart–Allmaras simulation technique.

In DDES model, the near wall region is modeled with a RANS approach where Reynolds Stresses term are modeled by SA model and the region at a certain distance from the wall the flow is treated with a LES approach where SubGrid Scale stresses are modeled by Smagorinsky model. So DDES model acts as a SA model close to the wall and distant from the wall as a SubGrid Scale (SGS) model which is a Smagorinsky model.

The SA model for the eddy viscosity involves a transport equation model in which a working variable $\tilde{\nu}$ is introduced to evaluate the turbulent viscosity and the eddy viscosity is defined by:

$$\nu_t = \tilde{\nu} f_{v1}$$

where f_{v1} is a damping function.

The Smagorinsky model is a subgrid scale model defines the eddy viscosity:

$$\nu_t = C_S h_K^2 |\nabla \mathbf{u}|$$

where C_S is a model constant.
The detailed of DDES model discussed in chapter 3.

2.8 Concluding Remarks

In this project we concentrate to implement and test the near wall boundary model with this simulation technique to investigate the effect of the boundary layer model and to the characterize the turbulent flow features efficiently.

Chapter 3

Near-Wall Turbulence Modeling and Implementation

The problem of predicting the behaviour of turbulent flows exists everywhere in engineering applications. LES that can accurately predict local spatial flow averages above a preassigned length scale, to be useful as an engineering design tool, needs enrichment of two fundamental problems [31]. First, better subgrid models are essential to deal with the delicate energy balance that must be integrated over long time intervals.

Second, betterment in boundary treatment of near wall turbulence is needed for complex geometries to achieve certain dynamic features, in which turbulence is the effect of interaction between the flow and the walls. These boundary treatments should not require full griding and resolution of turbulent boundary layers for using LES as a part of a design process in engineering applications.

So it is very important to model this turbulent boundary layer finding appropriate boundary conditions into the simulation concerning the required accuracy of LES turbulence simulation in the engineering settings. We have discussed two different techniques to model the near wall turbulent boundary layer which is entitled as near-wall modeling.

3.1 Introduction

Wall models are very important for enabling Large Eddy Simulations of realistic problems at high Reynolds numbers. Solving the "Near-Wall problems" requires essentially DNS type grid resolution in the innermost layer of turbulent boundary layers which prevents LES from being applied to many realistic turbulent flows [19].

A near wall modeling is necessary to model the inner part of the turbulent boundary layers into the LES simulation technique so that the LES technique can be used in the real engineering problems.

3.2 Numerical Simulations of wall bounded Turbulent Flows

Methodologies that are used into the numerical simulations of turbulent flows do not give accurate results in all flows without *ad hoc* adjustments of different types of problems.

In the RANS technique, equations are obtained by time- or ensemble-averaging the Navier–Stokes equations to get the transport equations for the averaged momentum. Then the effect of all the scales of motion is modeled. But no model appears to be accurate without specific adjustments of the model constants. The reason may be that the large, energy carrying eddies are much affected by the boundary conditions, and universal models of the motion may be impossible to develop [19].

In the DNS technique, all the scales of motion are resolved and the number of grid points in each direction is proportional to the ratio between the largest and the smallest eddy in the flow, which is $Re^{3/4}$ where Re is the Reynolds number based on an integral scale of the flow. So, for high Reynolds number engineering problems, it becomes more unrealistic using DNS. Due to the high computational cost of resolving all turbulent scales in the flow, DNS is limited to the moderate Reynolds number and simple geometry.

In the LES technique, large and energy carrying eddies are computed and the small, subgrid scales of motion are modeled, and the small scales tend to more isotropic and homogeneous than large scales. So concerning accuracy and computational cost LES technique is a powerful tool for real engineering applications.

For the wall bounded flows where turbulent eddies caused by the interaction of wall and flow, for the flows around a circular cylinder, LES technique needs to improve the treatment of the wall layer, so near wall modeling is implemented into the LES technique.

3.3 Near-Wall Turbulence Modeling

To model the near wall turbulent boundary layer using appropriate boundary conditions, there are two different classes of methods of near-wall modeling of turbulent boundary layers [21].

1. Hybrid LES/RANS and Delayed Detached Eddy Simulation (DDES)
2. Wall shear stress model

In first model, the unsteady evolution equations with the eddy viscosity are solved everywhere in the domain where in the inner layer the eddy viscosity is taken from some RANS type model and in the outer layer everywhere else in the flow the eddy viscosity is taken from some LES type subgrid model.

In the second model, the LES domain is defined as extending all the way to the wall, while an auxiliary set of equations is solved in an overlapping layer covering the innermost turbulent boundary layer. The exact wall boundary condition can be taken over directly for the normal velocity only and for the

other variables, a model is essential since they are not defined as surface mean values taken at the wall [23].

3.4 DDES Wall Model

A hybrid RANS/LES approach can be performed which is a single set of equations that blends RANS model and LES model into a generalized model and acts as a RANS model near the wall and transition to LES model where desired. For hybrid RANS/LES approaches a continuous treatment or smooth transition between RANS and LES model is important.

Simulation for massive separation is a significant field in which differences in approach can be observed deeply and a well deserve detailed discussion is possible. For high Reynolds number, massively separated flows remains, for which Detached Eddy Simulation (DES) is convincingly more competent than either unsteady Reynolds Averaged Navier Stokes(uRANS) or Large Eddy Simulation (LES) [27].

For pure LES technique the main objection is its computational cost. The boundary layer dominates for this computational cost even if we use wall modeling in LES [26]. For the RANS models it can be adjusted to predict boundary layers and their separation well but not large separation regions, whether behind a sphere or past bluff bodies and so on. Comparing these methods, DES is sufficiently efficient where the boundary layer is treated by RANS and the regions of massive separation are treated by LES and the regions between these areas known as the grey area, may be questionable unless the separation is abrupt which is often fixed by the geometry. So the approach DDES is considered to avoid the inadequacy of DES.

3.4.1 Detached Eddy Simulation

The Detached Eddy Simulation (DES) is a hybrid approach in which the small structures attached to the wall would be modeled in RANS mode whereas the larger ones populating the separated regions and wakes, i.e. detached to the wall would be resolved. So a single turbulence model functions as a subgrid scale model in regions where the grid density is fine enough for a LES and as a Reynolds averaged model in regions where it is not [1]. So the entire boundary layer is handled by RANS.

3.4.1.1 Formulation of DES approach

A DES model can be obtained by replacing a length scale d from a RANS model by a length proportional to a grid spacing Δ. Then the DES length scale, $\tilde{d}$, can be defined as:

$$\tilde{d} = \min(\mathrm{d}, \mathrm{C_{DES}}\Delta) \tag{3.1}$$

where C_{DES}, a modeling parameter which needs to be determined and Δ is the grid spacing defined as the largest of the spacing in all three directions:

$$\Delta = \max(\Delta_\mathrm{x}, \Delta_\mathrm{y}, \Delta_\mathrm{z}) \tag{3.2}$$

In the regions of the boundary layers grids are highly anisotropic ($\Delta_x \approx \Delta_y \gg \Delta_z$). Although typically the ratio between $(\Delta x \Delta y \Delta z)^{1/3}$ and d is unclear, $d \ll \Delta$ reduces the model to the standard RANS model. Conversely, if the grids are adequate to resolve the eddies which arise after massive separation, the grid cells are more isotropic and the eddy viscosity becomes grid dependent, and $\Delta \ll d$ so the model acts as a subgrid scale version of the RANS model.

Massive separation rapidly makes available a range of length scales much larger than the boundary layer thickness δ and dealing with this separation by DES is argued in the sense that the entire boundary layer thickness δ upstream of separation is handled by the RANS model ($\delta < C_{DES}\Delta$).

A primary concern is that the switch from RANS to LES mode is fixed by the grid according to equation (3.1) and a violation of the inequality $\delta < C_{DES}\Delta$ may occur due to the use of a very fine grid in both x and z directions.

A significant concern is the grey area, the region corresponding to $d \approx C_{DES}\Delta$ in which the behavior is not clear as the solution is neither pure RANS nor pure LES.

3.4.1.2 DES approach based on the SA model

The Spalart-Allmaras (SA) turbulence model solves one transport equation for the eddy viscosity which was used as a base model for the DES formulation. The two equation model in particular Shear Stress model (SST) was also used in some of the alternative approaches [28, 16].

The DES model is described here following from [18, p.256]:
The transport equation for the working variable $\tilde{\nu}$ is:

$$\begin{aligned}\frac{D\tilde{\nu}}{Dt} &= c_{b1}\tilde{S}\tilde{\nu} + \frac{1}{\sigma}[\nabla \cdot ((\nu + \tilde{\nu})\nabla\tilde{\nu}) + c_{b2}(\nabla\tilde{\nu})^2] \\ &\quad - c_{w1}f_w[\frac{\tilde{\nu}}{d}]^2\end{aligned} \tag{3.3}$$

where ν is the molecular viscosity, S is the magnitude of the vorticity, d is the distance to the nearest wall and expresses the confinement of the eddies by that wall and the transition terms were omitted. In the equation (3.3), the first part of the right hand side is the production term, second part is the diffusion term and the third part is the destruction term.

The Sub-Grid Scale (SGS) stresses are:

$$-\overline{u_i' u_j'} = \nu_t(\partial u_i/\partial x_j + \partial u_j/\partial x_i)$$

where u_i is the resolved field. The eddy viscosity ν_t in the case of Spalart DES model is evaluated by the relation based on the turbulent viscosity scale as,

$$\nu_t = \tilde{\nu} f_{v1}$$

where f_{v1} is a damping function defined as:

$$f_{v1} = \frac{\chi^3}{\chi^3 + c_{v1}^3}, \qquad \chi \equiv \frac{\tilde{\nu}}{\nu}$$

such that for the law of the wall, $\tilde{\nu} = Kyu_\tau$, $\tilde{S} = \dfrac{u_\tau}{Ky}$ in the log layer, in the buffer layer, and in the viscous sublayer where $K = 0.41$ is the von Kármán constant, y is the distance from the wall and u_τ is the shear stress velocity.

The vorticity magnitude S is modified such that the modified vorticity $\tilde{S}$ maintains its log-layer behaviour:

$$\tilde{S} = Sf_{v3} + \frac{\tilde{\nu}}{K^2 d^2} f_{v2}$$

where

$$f_{v2} = 1 - \frac{\chi}{1 + \chi f_{v1}}, \quad S = \sqrt{2\Omega_{ij}\Omega_{ij}} \quad \text{and} \quad f_{v3} = 1$$
$$\Omega_{ij} = \frac{1}{2}(\frac{\partial \tilde{u}_i}{\partial x_j} - \frac{\partial \tilde{u}_j}{\partial x_i})$$

A function f_w is introduced in order to obtain a faster decaying behaviour of the destruction term in the outer region of the boundary layer:

$$f_w(g) = g(\frac{1 + c_{w3}^6}{g^6 + c_{w3}^6})^{1/6}, \quad g = r + c_{w2}(r^6 - r), \quad r = \frac{\tilde{\nu}}{\tilde{S}K^2 d^2}$$

where g is a limiter that prevents large values of f_w, both r and f_w are equal to 1 in the log layer and decrease in the outer region.
The model constants are:

$$c_{b1} = 0.1355, \quad c_{b2} = 0.622, \quad \sigma = \frac{2}{3}, \quad K = 0.41$$
$$c_{w1} = \frac{c_{b1}}{K^2} + \frac{1 + c_{b2}}{\sigma}, \quad c_{w2} = 0.3, \quad c_{w3} = 2, c_{v1} = 7.1$$

The model contains a destruction term for its eddy viscosity, proportional to $(\tilde{\nu}/d)^2$ where d is the distance to the closest wall. When this term balanced with the production term, it adjusts the eddy viscosity to scale with local deformation rate $\tilde{S}$ and d:

$$\tilde{\nu} \sim \tilde{S}d^2$$

For the Smagorinsky model, it adjusts the subgrid scale eddy viscosity to scale with $\tilde{S}$ and the grid spacing Δ:

$$\nu_{SGS} \sim \tilde{S}d^2$$

So the model can be a subgrid scale model by replacing d with a length proportional to Δ. Thus we can replace d in the model destruction term by $\tilde{d}$, defined by

$$\tilde{d} = \min(\mathrm{d}, \mathrm{C_{DES}}\Delta) \tag{3.4}$$

If a local equilibrium is claimed between production and destruction term at the high Reynolds number limit, gives:

$$c_{b1} S \nu_t = c_{w1} f_w^{DES} (\frac{\nu_t}{C_{DES} \Delta})^2$$

leading to

$$\nu_t = \frac{c_{b1}}{c_{w1} f_w^{DES}} C_{DES}^2 \Delta^2 S \tag{3.5}$$

where f_w^{DES} can be determined as:

$$f_w^{DES} = g(f_w^{DES}) (\frac{1 + c_{w3}^6}{g(f_w^{DES})^6 + c_{w3}^6})^{1/6}$$

Equation (3.5) is analogous to the well known Smagorinsky model.

3.4.1.3 Modification of Standard SA-DES model

The standard Spalart-Allmaras RANS model can give unexpected distribution of eddy viscosity if the wall distance d in the model destruction term is replaced by $\tilde{d}$ in every equation. The damping functions into the model, may interpret the low eddy viscosity levels typical of resolved LES regions as closeness to the wall with corresponding subgrid viscosity.

Since the laminar suppression term f_{v2} (damping function) is included to the model to prevent spurious growth of small $\tilde{\nu}$, it is observed that for fully turbulent flows with adequately large free stream values inclusion of the laminar suppression term f_{v2} is effectively optional for negligible effect on the resulting flow.

As a modification, the near wall functions in the low Reynolds terms can be disabled only in the LES mode form DES:

$$f_{v1} = 1 \quad f_{v2} = 0 \quad f_w = 1 \tag{3.6}$$

But this equation (3.6) may lead to a discontinuity of ν_t at the RANS/LES interface due to the discontinuity of f_w compared to its RANS value. To prevent the activation of the low Reynolds terms in LES mode, the definition of the length scale can be redefined as an alternative approach, introduced in [18, p.260].

3.4.2 Delayed Detached Eddy Simulation

DES can have imprecise behaviour in thick boundary layers and shallow separation regions when the grid spacing parallel to the wall, Δ, becomes less than the boundary layer thickness,δ, i.e. $\Delta < \delta$, either through boundary grid refinement or boundary layer thickening. So even if the grid spacing is fine enough for the DES length scale to follow the LES branch, but there is possibility of lacking of LES content, called modeled stress depletion (MSD) and this depleted stresses reduce the skin friction, which can lead to premature separation [14].

But for a DES application, it is preferable to override the DES limiter and maintain RANS behavior in boundary layers, independent of wall parallel grid spacing relative to boundary layer thickness. For this reason, a modified version of DES is required which is referred as DDES.

3.4.2.1 Background

Separation is an important flow feature that motivates DES in which the boundary layer is treated with RANS and is quasi-steady, but the free shear layer it feeds develops LES content. If this switch form RANS to LES takes place very fast, it gives the better accuracy. But for standard DES on typical grids, this switch is not very fast at all. So several approaches developed, modified from DES, such as Zonal Detached Eddy simulation (zonal DES), Delayed Detached Eddy simulation (DDES) and Improved Delayed Detached Eddy simulation (IDDES).

We focus on DDES approach, the solution process determines the separation. It detects the boundary layers and makes longer the full RANS mode, even if the wall parallel grid spacing activates the DES limiter. As this detection depends on the eddy viscosity, the limiter depends on the solution [14].

3.4.2.2 Review of DDES approaches

The formulation for DDES is designed, based on Spalart–Allmaras DES, by redefining the DES length scale $\tilde{d}$ as:

$$\tilde{d} = d - f_d \max(0., \mathrm{d} - \mathrm{C_{DES}}\Delta) \tag{3.7}$$

where f_d is a shielding function designed by the quantity r_d.

Setting f_d to 0 yields RANS ($\tilde{d} = d$) no matter how fine the grid is, while setting it to 1 gives standard DES ($\tilde{d} = \min(\mathrm{d}, \mathrm{C_{DES}}\Delta)$).

The approach DDES involves a parameter r_d which is slightly modified relative to the Spalart-Allmaras definition so that can be applied to any eddy viscosity model and slightly more robust in irrotational regions:

$$r_d = \frac{\nu_t + \nu}{\sqrt{U_{i,j}U_{i,j}}K^2 d^2}, \quad K = 0.41 \tag{3.8}$$

where ν_t is the kinematic eddy viscosity, ν is the molecular viscosity, $U_{i,j}$ the velocity gradients, d the distance to the wall and K is the von Kármán constant.

This is a slightly modified version of the parameter $r = \dfrac{\tilde{\nu}}{\tilde{S}K^2 d_w^2}$ appearing in the SA model which represent the ratio (squared) of the model integral length scale to the distance to the wall.

This parameter r_d equals 1 in a logarithmic layer and falls to 0 gradually towards the edge of the boundary layer. The addition of ν in the numerator ensures that r_d remains away from 0 so that the behavior of very near wall is well defined.

Now using this quantity, r_d, the delaying function, f_d, in equation (3.7), can be defined as:

$$f_d = 1 - \tanh([8r_d]^3) \tag{3.9}$$

which is designed to be 1 in the LES region, where $r_d \ll 1$, and 0 elsewhere and to be insensitive to r_d exceeding 1 very near the wall.

The DDES length scale does not depend only on the grid but depends also on the time-dependent eddy viscosity field. From the practical applications, it can be observed that the RANS mode is maintained in thick boundary layers whilst maintaining LES content after separation.

3.4.3 Implementation of DDES Wall Model

We model the near wall turbulent layer in the spirit of DDES model, consists of the coupling of the LES model with a subgrid model in the near wall region. The design of such hybrid RANS/LES models would ideally allow to compute large scale instabilities while being able to model turbulence stresses in using subgrid scale functions in zones where the local mesh size h_K is considerably smaller than δ_t the thickness of the turbulent boundary layer:

$$\eta_{DES}(\mathbf{x}) = \min_{\mathbf{x}\in\Omega}\big(\eta_{RANS}(\mathbf{x}), C_{DES}\eta_{LES}(\mathbf{x})\big) \tag{3.10}$$

with C_{DES} a model constant.

Thus in the near-wall region, $\eta_{LES} >> \eta_{RANS}$ as the mesh size is higher than the dissipative scale in the boundary layer if one assumes that $C_{DES}\, h_K > \delta_t$ then the model degenerates the RANS, while in the inner region $\eta_{DES} = C_{DES}\eta_{LES}$.

The SGS stresses are given by $-\overline{u_i' u_j'} = \nu_t(\partial u_i/\partial x_j + \partial u_j/\partial x_i)$ where u_i is the resolved field. For instance, the eddy viscosity η_{RANS} in the case of the Spalart DES model is based on the turbulent viscosity scale $\tilde{\nu}$ evaluated by the relation,

$$\eta_{RANS} = \tilde{\nu} f_{\nu 1}(\tilde{\nu}) \tag{3.11}$$

where $\tilde{\nu}$ is the turbulent viscosity solution to the Spalart–Allmaras equation and $f_{\nu 1}$ is a damping function defined such that the Kármán profile $\nu_t/\nu \sim \kappa y^+$ is enforced in the near-wall region.

The LES viscosity is the Smagorinsky viscosity, for any cell $K \in \mathcal{M}$,

$$\eta_{LES}(K) = C_S h_K^2 |\nabla \mathbf{u}| \tag{3.12}$$

The model depends on several empirical constants which might be changed depending on the Reynolds number and the geometry of the problem.

3.4.4 Remarks

MSD and Grid Induced Separation (GIS) are the most significant practical issues and worse to deal with the original DES. If the grid spacing is small enough for the viscosity to be affected by the DES limiter but not small enough

to support accurate LES content, MSD takes place and a consequence of MSD is GIS. GIS could be viewed as an early separation even if the solution is steady and accurate but as with the model it becomes grid dependent [27].

In the original DES, there was no adjustments to the log layers in the boundary wall layer so log layers were miss aligned, called as logarithmic layer mismatch. So the control between RANS and LES is not fully understood of hybrid RANS/LES method.

DDES approach works well with the wall parallel grid spacing less than the boundary layer thickness and in [14] this approach was validated for a flat plate with grid spacing, 1/10 of the boundary layer thickness.

3.5 Wall Shear Stress Model

Wall shear stress model, a near wall modeling for turbulent wall layer of turbulent flows in a complex geometries can be written in the following form:

If we divide a bounded domain $\Omega \subset \mathbb{R}^d$ with $d = 2, 3$ into the boundaries $\partial\Omega = \Gamma_{\text{infl}} \cup \Gamma_{\text{slfpr}} \cup \Gamma_{\text{outfl}}$ so that the parts are mutually disjoint, then the slip with linear friction and penetration with resistance boundary conditions are applied on Γ_{slfpr} can be defined by:

$$u \cdot n + \alpha n^T \sigma n = 0 \quad \text{on} \quad \Gamma_{\text{slfpr}} \tag{3.13}$$

$$u \cdot \tau_k + \beta^{-1} n^T \sigma \tau_k = 0, \quad \text{on} \quad \Gamma_{\text{slfpr}} \quad 1 \leq k \leq d-1 \tag{3.14}$$

where σ is the shear stress, n is an outer normal vector on $\partial\Omega$, τ_k orthogonal unit tangent vectors at the boundary, α a penetration parameter and β a skin friction parameter are piecewise constant on the boundary Γ_{slfpr} and β is chosen based on the Reynolds number and the roughness of the boundary also as a function of space and time similar to simple wall shear stress models [19, 23].

If we consider $\alpha \to 0$, we get no penetration condition and $\alpha \to \infty$ gives free penetration condition. If we choose no penetration condition into (3.13), then the condition $\beta \to 0$ in (3.14) gives free slip boundary conditions and $\beta \to \infty$ prescribes no slip conditions.

We consider in this project no penetration condition:

$$u \cdot n = 0 \quad \text{on} \quad \Gamma_{\text{slfpr}} \tag{3.15}$$

$$u \cdot \tau_k + \beta^{-1} n^T \sigma \tau_k = 0, \quad \text{on} \quad \Gamma_{\text{slfpr}} \quad 1 \leq k \leq d-1 \tag{3.16}$$

The slip boundary condition on Γ_{slfpr} describes that the normal velocity is zero on the boundary *i.e.* the pressure is the only nonzero flux on the given boundary Γ_{slfpr}.

3.5.1 Implementation of wall shear stress model

3.5.1.1 weak implementation

The tangential components (friction) *i.e.* slip with friction boundary condition in (3.16) is implemented in the weak form by adding boundary integrals in the variational form (2.2). So the weak form with the boundary integrals is:

$$\int_Q \dot{u}\cdot v + \int_Q (u\cdot\nabla u).v + \int_Q \sigma\nabla\cdot v - \int_{\Gamma_{\text{slfpr}}\times I} \sigma v\cdot n - \int_Q f.v = 0$$
$$\int_Q \nabla\cdot u\cdot q = 0 \tag{3.17}$$

where $\int_{\Gamma_{\text{slfpr}}\times I}\sigma v\cdot n = \int_{\Gamma_{\text{slfpr}}\times I}\sigma v\cdot n ds dt$. We decompose the test function v on Γ_{slfpr} into d orthonormal components:

$$v = (v\cdot n)n + \sum_{k=1}^{d-1}(v\cdot\tau_k)\tau_k \tag{3.18}$$

Then the boundary integral in the variational formulation can be rewritten:

$$\int_{\Gamma_{\text{slfpr}}\times I}\sigma n\cdot v = \int_{\Gamma_{\text{slfpr}}\times I} n^T\sigma n(v\cdot n) + \int_{\Gamma_{\text{slfpr}}\times I}\sum_{k=1}^{d-1} n^T\sigma\tau_k(v\cdot\tau_k)$$

Then implementing the normal and the tangential components of boundary conditions from equations (3.13) and (3.14) we rewrite the variational formulation of the boundary integral:

$$\int_{\Gamma_{\text{slfpr}}\times I}\sigma n\cdot v = \int_{\Gamma_{\text{slfpr}}\times I}\alpha^{-1}(u.n)(v.n) - \int_{\Gamma_{\text{slfpr}}\times I}\sum_{k=1}^{d-1}\beta(u\cdot\tau_k)(v\cdot\tau_k)$$

Applying the normal and the tangential components condition, the weak form (3.17) with the boundary integrals is:

$$\int_Q \dot{u}\cdot v + \int_Q (u\cdot\nabla u).v + \int_Q \sigma\nabla\cdot v - \int_{\Gamma_{\text{slfpr}}\times I}\alpha^{-1}(u.n)(v.n)$$
$$+\int_{\Gamma_{\text{slfpr}}\times I}\sum_{k=1}^{d-1}\beta(u\cdot\tau_k)(v\cdot\tau_k) - \int_Q f.v = 0$$
$$\int_Q \nabla\cdot u\cdot q = 0$$

The time and space discretization of this weak form with the boundary integrals where slip with friction boundary condition and penetration with resistance applied can be written in the following form form the the equation (2.5):

$$((U^n - U^{n-1})k_n^{-1} + \widehat{U}^n\cdot\nabla\widehat{U}^n, v) + (2\nu\epsilon(\widehat{U}^n),\epsilon(v)) - (P^n,\nabla\cdot v) + (\nabla\cdot\widehat{U}^n, q)$$
$$-\int_{\Gamma_{slfpr}}(\sigma(U^n,P^n)\cdot n).v ds = (f,v) \qquad \forall\hat{v} = (v,q)\in V_0^n\times W^n$$

implies,

$$((U^n - U^{n-1})k_n^{-1} + \widehat{U}^n\cdot\nabla\widehat{U}^n, v) + (2\nu\epsilon(\widehat{U}^n),\epsilon(v)) - (P^n,\nabla\cdot v) + (\nabla\cdot\widehat{U}^n, q)$$
$$-\int_{\Gamma_{\text{slfpr}}\times I}\alpha^{-1}(\widehat{U}^n.n)(v.n) + \int_{\Gamma_{slfpr}}\sum_{k=1}^{d-1}\beta(\widehat{U}^n\cdot\tau_k)(v\cdot\tau_k)ds = (f,v)$$
$$\forall\hat{v} = (v,q)\in V_0^n\times W^n$$

where $V_0^n\times W^n$ is defined in 2.5.3. If we consider no penetration conditions, then the boundary integral with penetration parameter vanishes and pure slip condition and slip with friction boundary conditions remain only, that we focused on here.

3.5.1.2 Strong implementation

For the strong implementation of Wall Shear Stress Model, the normal component condition *i.e.* slip boundary condition (3.15) is applied after assembling the stiffness matrix and the right hand side vector (called load vector) by modifying the algebraic system.

To modify the algebraic system, the row of the stiffness matrix and load vector corresponding to a boundary vertex is replaced by a new row according to the boundary condition, implemented according to [17].

To implement slip and slip with friction boundary condition strongly, the test function v is initially defined in the Cartesian standard basis vector (e_1, e_2, e_3). Then, the normal-tangent coordinate systems are defined for the vertices on the boundary with the basis vector (n, τ_1, τ_2), where $n = (n_1, n_2, n_3)$ is the normal and $\tau_1 = (\tau_{11}\tau_{12}\tau_{13})$, $\tau_2 = (\tau_{21}\tau_{22}\tau_{23})$ are tangents to each vertex on the boundary so that the test function can be mapped locally to these normal-tangent coordinates.

The test function v is decomposed as (3.18) in which the normal-tangent coordinate system allows us to let the normal direction to be constrained and the tangent directions be free *i.e.* the rows of the matrix and the load vector corresponding to the boundary is multiplied with n, τ_1, τ_2, respectively, and added together, and then the normal velocity is set to 0.

3.5.1.3 Implementation of Slip Boundary Condition

For implementing the slip boundary condition, the normal and tangent vectors (n, τ_1, τ_2) are computed on the boundary vertices, following [12] and then the modification of the algebraic system is done after assembling the stiffness matrix and the load vector, following [17].

To compute the normal and tangent vectors on the boundary vertices, based on the different positions of the vertex on the boundary, we divide the boundary vertices of the computational domain into three different node types for 3D problems. The node types are:

1. node type 1 - node is on a surface ; apply slip boundary condition
2. node type 2 - node is on a edge ; apply slip boundary condition
3. node type 3 - node is on a corner ; apply no slip boundary condition

But for 2D problems, the node types are defined:

1. node type 1 - node is on a surface ; apply slip boundary condition
2. node type 2 - node is on a corner ; apply no slip boundary condition

3.5.1.4 Computation of tangent and normal vectors

Computation for 2D problems

For $d = 2$ in (3.18), for node type 1, the only tangential vector is τ_1, which is defined by $\tau_1 = (-n_2, n_1)^T$. For node type 2, we apply no slip boundary condition at the corner.

Computation for 3D problems

For $d = 3$ in (3.18), the tangential vectors are τ_1, τ_2, span the tangential plane such that $\{n, \tau_1, \tau_2\}$ is a system of orthonormal vectors.

For node type 1 , if the absolute values of the angles between the facet normals are less than the maximum angle > 0 then the facets are defined to belong to the same surface. We choose the maximum angle $\frac{\pi}{2}$. To compute a normal to a vertex for each surface, a weighted average of all the facet normals which contain the vertex is calculated and the weights for each facets are calculated as the area of the facet.

Tangential vectors are computed with the normal vectors given for each facet of an element. If $n = (n_1, n_2, n_3)$ is the normal vector given with the Euclidean norm $\|n\|_2$, then there is at least one component n_i with $|n_i| \geq 0.5$. The computation of τ_1 and τ_2 for node type 1 is represented in the algorithm 1 introduced in [12].

Algorithm 1 Computation of $\tau_1 = (\tau_{11}, \tau_{12}, \tau_{13})$ and $\tau_2 = (\tau_{21}, \tau_{22}, \tau_{23})$for node type 1 [12]

if ($|n_1| \geq 0.5$ OR $|n_2| \geq 0.5$) **then**
  $n := \sqrt{{n_1}^2 + {n_2}^2}$
  $\tau_{11} := n_2/n$
  $\tau_{12} := -n_1/n$
  $\tau_{13} := 0$
  $\tau_{21} := -\tau_{12} n_3$
  $\tau_{22} := \tau_{11} n_3$
  $\tau_{23} := \tau_{12} n_1 - \tau_{11} n_2$
else
  $n := \sqrt{{n_2}^2 + {n_3}^2}$
  $\tau_{11} := 0$
  $\tau_{12} := -n_3/n$
  $\tau_{13} := n_2/n$
  $\tau_{21} := \tau_{13} n_2 - \tau_{12} n_3$
  $\tau_{22} := -\tau_{13} n_1$
  $\tau_{23} := \tau_{12} n_1$
end if

The two cases in algorithm 1 ensures that a division by zero never takes place.

For node type 2, a vertex belongs to an edge or to the two surfaces. To compute the normal and tangential vectors, normals are computed form the first surface as vector n and from the second surface as vector τ_2 and τ_2 is calculated form the surface normals $\mathrm{sn}[i] = \mathrm{sn}[i]_1, \mathrm{sn}[i]_2, \mathrm{sn}[i]_3$ of the second surface where $i =$ node type $- 1$ and n. Then the tangential vector τ_1 at the edge is computed by taking the cross product of n and τ_2, $\tau_1 = n \times \tau_2$. The computation of τ_1 and τ_2 for node type 2 is presented in the algorithm 2.

Algorithm 2 Computation of $\tau_1 = (\tau_{11}, \tau_{12}, \tau_{13})$ and $\tau_2 = (\tau_{21}, \tau_{22}, \tau_{23})$ for node type 2

if node type2 **then**
  $\tau_{21} := n_2 \mathrm{sn}[i]_3 - \mathrm{sn}[i]_2 n_3$
  $\tau_{22} := n_3 \mathrm{sn}[i]_1 - \mathrm{sn}[i]_3 n_1$
  $\tau_{23} := n_1 \mathrm{sn}[i]_2 - \mathrm{sn}[i]_1 n_2$
  $\tau_{\mathrm{norm}} := \sqrt{{\tau_{21}}^2 + {\tau_{22}}^2 + {\tau_{23}}^2}$
  $\tau_{21} := \tau_{21}/\tau_{\mathrm{norm}}$
  $\tau_{22} := \tau_{22}/\tau_{\mathrm{norm}}$
  $\tau_{23} := \tau_{23}/\tau_{\mathrm{norm}}$
  $\tau_{11} := \tau_{22} n_3 - \tau_{23} n_2$
  $\tau_{12} := \tau_{23} n_1 - \tau_{21} n_3$
  $\tau_{13} := \tau_{21} n_2 - \tau_{22} n_1$
end if

For node type 3, a vertex belongs a corner or to more than two surfaces. We find the normal and tangential vectors in a similar style of type 2.

3.5.1.5 Modification of Algebraic System

To apply slip boundary condition on different types of boundary nodes, we do a local coordinate mapping from the Cartesian to the normal-tangent coordinate system and as this mapping is done locally only for the nodes on the boundary, so to modify the the algebraic system only the corresponding rows changes and the other rows remain the same.

We assume that from the variational form we finish up with an algebraic system of a matrix-vector form $A\hat{u}(K_l) = b$ where K_l is the set of all degrees of freedom (dof), A is a stiffness matrix and b is a load vector. And to modify this algebraic system, the dofs are enumerated in the following manner: The first Cartesian component dof of the momentum are enumerated from 1 to N, the second Cartesian component dof from 1+N to 2N, the third Cartesian component dof from 1+2N to 3N and the stiffness matrix is of a $(3N, 3N)$ matrix. Now, we also assume that $i \in K_l$ is a boundary node where we need to enforce the slip boundary condition, implemented as in [17].

$$\begin{pmatrix} \cdots & \cdots & \cdots & \cdots & \cdots & \cdots & \cdots \\ \cdots & a_{i+N,i+N} & \cdots & a_{i+N,i+2N} & \cdots & a_{i+N,i+3N} & \cdots \\ \cdots & \cdots & \cdots & \cdots & \cdots & \cdots & \cdots \\ \cdots & a_{i+2N,i+N} & \cdots & a_{i+2N,i+2N} & \cdots & a_{i+2N,i+3N} & \cdots \\ \cdots & \cdots & \cdots & \cdots & \cdots & \cdots & \cdots \\ \cdots & a_{i+3N,i+N} & \cdots & a_{i+3N,i+2N} & \cdots & a_{i+3N,i+3N} & \cdots \\ \cdots & \cdots & \cdots & \cdots & \cdots & \cdots & \cdots \end{pmatrix} \cdot \begin{pmatrix} \cdots \\ {u^1}_i \\ \cdots \\ {u^2}_i \\ \cdots \\ {u^3}_i \\ \cdots \end{pmatrix} = \begin{pmatrix} \cdots \\ b_{i+N} \\ \cdots \\ b_{i+2N} \\ \cdots \\ b_{i+3N} \\ \cdots \end{pmatrix} \tag{3.19}$$

To modify the algebraic system for 3D problem, we first assume that r1, r2, r3 are the rows of the matrix-vector form that correspond to the boundary nodes. For the case of node type 1, the vertices belong to a surface and we

put the normal velocity to zero to apply the slip boundary condition for these vertices. So the row r1 into matrix A is replaced by the normal components n and the rows r2 and r3 are changed by applying the normal components τ_1 and τ_2 to the elements of r2 and r3 and and the corresponding row r1 in to the load vector b is put to zero. So the stiffness matrix A and the load vector b take the form:

$$\begin{pmatrix} \cdots & \cdots & \cdots & \cdots & \cdots & \cdots & \cdots \\ 0 & n_1 & 0 & n_2 & 0 & n_3 & 0 \\ \cdots & \cdots & \cdots & \cdots & \cdots & \cdots & \cdots \\ \cdots & {a'}_{i+2N,i+N} & \cdots & {a'}_{i+2N,i+2N} & \cdots & {a'}_{i+2N,i+3N} & \cdots \\ \cdots & \cdots & \cdots & \cdots & \cdots & \cdots & \cdots \\ \cdots & {a''}_{i+3N,i+N} & \cdots & {a''}_{i+3N,i+2N} & \cdots & {a''}_{i+3N,i+3N} & \cdots \\ \cdots & \cdots & \cdots & \cdots & \cdots & \cdots & \cdots \end{pmatrix} \cdot \begin{pmatrix} \cdots \\ {u^1}_i \\ \cdots \\ {u^2}_i \\ \cdots \\ {u^3}_i \\ \cdots \end{pmatrix} = \begin{pmatrix} \cdots \\ 0 \\ \cdots \\ {b'}_{i+2N} \\ \cdots \\ {b''}_{i+3N} \\ \cdots \end{pmatrix} \tag{3.20}$$

where

$$\begin{aligned} {a'}_{i+2N,j} &= a_{i+N,j}\tau_{11} + a_{i+2N,j}\tau_{12} + a_{i+3N,j}\tau_{13} \qquad j = 1, 2, \cdots, 3N \\ {b'}_{i+2N} &= b_{i+N}\tau_{11} + b_{i+2N}\tau_{12} + b_{i+3N}\tau_{13} \end{aligned}$$

and

$$\begin{aligned} {a''}_{i+3N,j} &= a_{i+N,j}\tau_{21} + a_{i+2N,j}\tau_{22} + a_{i+3N,j}\tau_{23} \qquad j = 1, 2, \cdots, 3N \\ {b''}_{i+3N} &= b_{i+N}\tau_{21} + b_{i+2N}\tau_{22} + b_{i+3N}\tau_{23} \end{aligned}$$

For node type 2 the boundary vertex belong to a edge and we apply slip boundary condition and we put the normal velocity to zero So the rows r1 and r2 into matrix A are replaced by the normal components n and τ_1 and the row r3 is changed by applying the normal component τ_2 to the elements of r3 and and the corresponding rows r1 and r2 in to the load vector are put to zero. So the stiffness matrix A and the load vector b take the form:

$$\begin{pmatrix} \cdots & \cdots & \cdots & \cdots & \cdots & \cdots & \cdots \\ 0 & n_1 & 0 & n_2 & 0 & n_3 & 0 \\ \cdots & \cdots & \cdots & \cdots & \cdots & \cdots & \cdots \\ 0 & \tau_{11} & 0 & \tau_{12} & 0 & \tau_{13} & 0 \\ \cdots & \cdots & \cdots & \cdots & \cdots & \cdots & \cdots \\ \cdots & {a''}_{i+3N,i+N} & \cdots & {a''}_{i+3N,i+2N} & \cdots & {a''}_{i+3N,i+3N} & \cdots \\ \cdots & \cdots & \cdots & \cdots & \cdots & \cdots & \cdots \end{pmatrix} \cdot \begin{pmatrix} \cdots \\ {u^1}_i \\ \cdots \\ {u^2}_i \\ \cdots \\ {u^3}_i \\ \cdots \end{pmatrix} = \begin{pmatrix} \cdots \\ 0 \\ \cdots \\ 0 \\ \cdots \\ {b''}_{i+3N} \\ \cdots \end{pmatrix} \tag{3.21}$$

where

$$\begin{aligned} {a''}_{i+3N,j} &= a_{i+N,j}\tau_{21} + a_{i+2N,j}\tau_{22} + a_{i+3N,j}\tau_{23} \qquad j = 1, 2, \cdots, 3N \\ {b''}_{i+3N} &= b_{i+N}\tau_{21} + b_{i+2N}\tau_{22} + b_{i+3N}\tau_{23} \end{aligned}$$

For the case of node type 3 in 3D and of node type 2 in 2D where the boundary vertex belongs to a corner, the velocity in all directions is constrained to zero and same as the zero velocity boundary condition *i.e.* no slip boundary

condition for this vertex. So we replace the row by an identity vector and the load vector is set zero.

Finally, to get the largest elements on the diagonal of the matrix, we find the maximum component of the normals that is replaced directly and of the elements that is replaced after applying the normal components to the elements. So we get the rows of the matrix re-arranged in which the largest matrix elements are on the diagonal to assure the good conditioning of the matrix.

3.5.2 Remarks

To compute the node normals we take a weighted average of the surrounding facet normals. And we identify the edges and corners from the angles between facet normals for which the velocity is constrained in 2 and 3 linearly independent directions respectively. So there may come the artificial constraining velocities for the mesh constructing near rounded surface of sharp radius. To avoid this artificial velocities near rounded surface of sharp radius, special care needs to be taken.

3.6 Concluding Remarks

We reviewed both the near-wall models discussed here with different boundary layer interaction problems which lead to the significant flow characteristics, separation and reattachment length of the turbulent boundary layer to identify the effects of the near wall modeling into the large eddy simulation technique. In this project, Wall Shear Stress Model is taken as near wall turbulence modeling for the sensitivity analysis of the near wall turbulence model into the simulation.

Chapter 4

Analysis of Separation and Reattachment Length

Separation and reattachment are two significant features for high Reynolds number turbulent flows in complex geometries and to characterize these features, different models of near wall modeling have been used in turbulent simulation. To analyze the efficiency and accuracy of the near wall models, it is important to characterize these features: separation and reattachment length.

4.1 Introduction

We study the physical phenomena associated with separated flows, to understand the effects of the turbulence modeling to separation.

4.1.1 Physical phenomena of Separated Flows

Separation describes the entire process in which a flow detaches from a solid surface and as a result a breakdown of the boundary layer occurs. The boundary layer undergoes a sudden thickening and causes an increased interaction between the viscous-inviscid layers.

In 2D, the flow velocity responds by decelerating if the pressure increases along the primary flow direction and, eventually will come to zero and a reversal of the flow will occur if this pressure differential continues.

The location at which flow reversal takes place, varies along the wall and this flow reversal at a described location in the vicinity of separation, may develop only a fraction of total time. Since the flow is not fully separated at these locations, said to be intermittent.

The flow locations were defined quantitatively based on the fraction of time that the flow moves downstream: incipient detachment (location where flow reversal takes place 1% of the time), intermittent transitory detachment (flow reversal takes place 20% of the time), transitory detachment (flow reversal occurs 50% of time) and detachment (where averaged wall shearing stress is zero) [25]. The location and distance between each of these positions depends on the flow parameters and geometry.

4.2 Analysis of Separation

For slightly viscous incompressible turbulent flows at high Reynolds number, the tangential forces or skin friction forces on the surfaces are small and both drag and lift forces comes mainly from the pressure forces, so particularly the pressure distribution at the turbulent separation is significant for the flow analysis.

4.2.1 Computation of Separation

In 2D, flow separation occurs when a positive pressure gradient *i.e.* an adverse pressure gradient begins to retard upon the flow. So the point of separation can be defined where the velocity reduces to zero or negative at the wall and the boundary layer thickens. The wall shear stress at the point of separation on the wall becomes zero because of the continuous retardation of flow by adverse pressure gradient.

4.2.2 Remarks

A wall shear stress model that uses the slip with friction boundary condition can model the flow separation corresponding to the transition from laminar to a turbulent boundary layer (drag crisis) by varying the skin friction parameter of the wall shear stress model. A pure slip boundary condition $\beta = 0$ can give accurate model of flow separation for many applications in aerodynamics.

4.3 Analysis of Reattachment

Separation from two dimensional sharp edged bluff bodies and reattachment is hard to study since the major detachment occurs near the sharp edges of the body with accompanying large variations in velocity and pressure around the detachment location [25].

The flow downstream of detachment is mainly dependent upon the upstream velocity distribution and the local geometry of the surface around the detachment location, and the thickness of the energetic outer region flow is comparable in size to that of the backflow region. The recirculating zone of the fluid flow is a significant portion of the entire detached shear layer. The turbulent shear layer reattaches to the surface with an adjacent in the near wake at some distance downstream.

For flows in a step channel, the upstream boundary layer detaches at the sharp corner which forms a free shear layer. The transition begins soon after the detachment if the boundary layer is laminar, unless the Reynolds number is very low. The separated shear layer curves sharply downward in the reattachment zone and collides on the wall, and part of the shear layer fluid is deviated upstream into the recirculating flow by a strong adverse pressure gradient.

4.3.1 Computation of Reattachment

We will study the position of the reattachment point of a recirculating vortex behind the step for flows in a channel across the step as recirculating vortex is

a distinctive feature of these flows. We study the dependency of position of this reattachment point on the value of the model parameter of different near wall turbulence model.

For computing reattachment point in 2D domain, we compute the tangential velocity on the bottom boundary since it does not vanish due to slip with friction boundary condition. Then the reattachment point is defined by the change of the sign of the tangential velocity and the tangential velocity is negative to the left of the reattachment point and positive to the right of the point because of the recirculation vortex.

4.3.2 Remarks

We study the effect of the near wall turbulence modeling to the simulation by computing reattachment point as it is a significant feature of flows in a channel across a step.

4.4 Concluding Remarks

Analysis of separation and reattachment are the important flow features for bluff bodies or circular structures and we study these phenomena of flows to understand the effect of the different near wall turbulence models in the simulation techniques and characterize the flow fields with significant accuracy. Separation is important in many engineering applications such as for the stall prediction of airfoils and wings, to predict the performance characteristics of turbo-machinery components, to predict the pressure losses in diffusers.

Chapter 5

Case Study I : Flow Across a Step Channel

We use the wall shear stress model [9] to model the turbulent boundary layers, described in chapter 3. Numerical studies for flows in different test problems are presented. To study the sensitivity analysis of the wall shear stress model to the simulation technique, we studied the dependency of different outputs of interest on different model parameters of wall model. The influence of the friction parameter of wall shear stress model to the flow field is analyzed and the results are discussed according to the physics of the flow.

5.1 Test Problem

To understand the flow behaviour and characterize the sensitivity of the model parameters to the results, we studied different types of test problems with different flow features. We analyzed the results which are most distinctive flow features such as reattachment length of recirculating vortex, turbulent flow separation to study the sensitivity of wall model.

We investigate the sensitivity of model parameters of near wall model to the simulation techniques, so it is very important to have a systematic study of the effects of the near wall model in well defined test problems.

We present the numerical studies for flows in a channel across a step since recirculation of a flow is a very natural situation. To analyze the effects of friction parameter of near wall model to the flow features, we considered the test case as a two dimensional problem.

5.1.1 Motivation of the Test Problem

We have chosen one of our test problem flow across a step channel inspired by its physical realization. Since this test problem is geometrically simple and do not scale with the Reynolds number [15, p. 236], so it is a very good test problem for numerical studies. This is a well defined test problem because the flow fields possess certain distinctive flow features such as recirculating vortex exists for the flows into the channel across a step.

5.1.2 Applications of the Test Problem

The study of the test problem flow across a step channel in which recirculating vortex is an important flow feature, helps to analyze fluid dynamics in the real engineering applications, as recirculating vortex is common in many engineering problems. So applications of studying the test problem flow across a step channel are involved in the scope of wind engineering and many fluid devices, such as weirs, gas turbines, turbo machines and combustion ducts.

5.2 Flow across a step channel

For turbulent flow simulations, it is important to keep track the details of the three effects : generation of eddies at walls, interaction of eddies and decay of eddies since all the vorticity is generated at boundary for the case of flows with potential body surface and laminar initial conditions [31]. For turbulent flows, to capture the generation of eddies at the boundary, wall models used into the simulation techniques play important role.

We consider the flows across a step channel as the recirculating vortex behind the step is the most significant feature of these flows. We investigate the flows with recirculating vortex caused by the flow boundary interaction using the wall shear stress model.

For recirculating flows, large differences between the reference velocities in the free stream and in the recirculation region are observed usually. A sensitivity analysis on the output results for different model parameters and a convergence analysis for the results is done in this section. A sensitivity based analysis is performed to analyze the dependency of the position of the reattachment point in 2D of these recirculating vortex on the value of the friction parameter β.

5.3 Test Case I: Two Dimensional Flow Across a Step Channel

For flows in a two dimensional channel with a step, recirculating vortex appears behind the step and we compute the reattachment length of the recirculating vortex. The tangential velocity on the bottom boundary of the step channel does not disappear because of the boundary conditions specified, so the reattachment point can be defined by the change of the sign of the tangential velocity in which tangential velocity is negative to left of the reattachment point and positive to the right [12].

Geometry Specifications

The geometry of the domain of a two dimensional channel flow across a step is used in the computation presented in Figure 5.1. The same domain was used in computations in [32] in order to simulate the experiments of separated Stokes flow by Taneda [29].

An inflow boundary condition specified on the left boundary Γ_{infl} of the domain, an outflow boundary condition Γ_{outfl} where the flow leaves which we

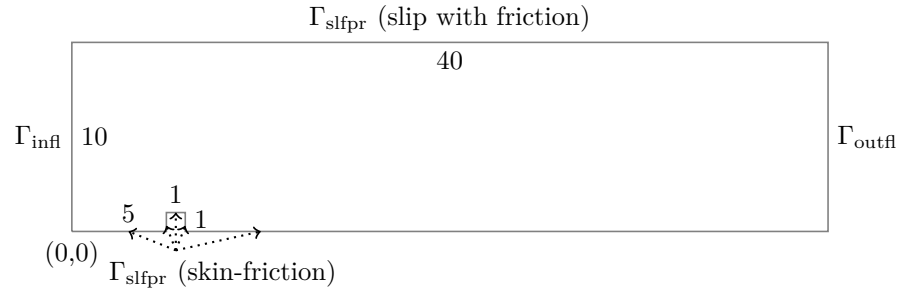

Figure 5.1: Geometry for two dimensional channel flow across a step

say a “do nothing" boundary 2.4 on the right boundary of the domain, a slip with friction boundary condition on the top and on the bottom boundary of the domain different boundary conditions are prescribed as different test case: no slip boundary condition, perfect slip boundary condition and slip with skin friction boundary condition, Figure 5.1.

The results for a parabolic and a constant inflow profile as the inflow boundary conditions are analyzed.

Mesh Generation

We performed our simulations with the initial grid (level 0) presented in Figure 5.2, similar to the grid presented in [12] as we can compare our results with his results taking as a benchmark result. Initially, for level 0, the horizontal grid lines are set at $y \in \{1, 2.5, 5\}$ and the vertical grids at $x \in \{5/3, 10/3, 5, 6,$-$7.785, 10.25, 14.5, 18.75, 23, 27.25, 31.5, 35.75\}$ to generate the higher level computational grids for the numerical studies.

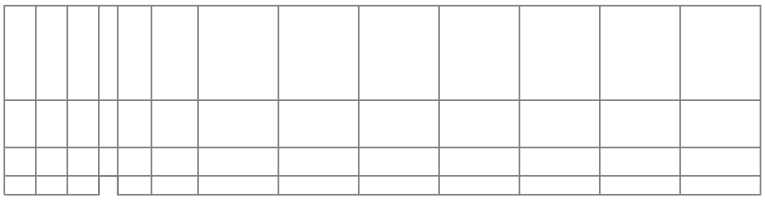

Figure 5.2: Computational grid (level 0) for two dimensional channel with a step

The resulting degrees of freedom for finer levels are given in Table 5.1. The higher levels of computational grid are generated by the dolphin mesh generation where initially level 0 grid are used as an input and in our simulation we have used the method which is not adaptive.

Table 5.1: Degrees of freedom for the two dimensional flow across a step

Level	total
0	140
3	6818
4	26690
5	105602

We run the simulation for these different grid levels and analyze the results.

Model Parameters

The details of the computational parameters are summarized in Table 5.2 where Time Iterator is the end time of the simulation, pde:viscosity means the viscosity, wall bc for defining the wall boundary condition, and solver::equation residual tol is to define the residual tolerance of our solver. We take wall boundary condition as a model parameter where wall boundary conditions are defined into our wall shear stress model.

Table 5.2: Computational parameters used in the simulation

Parameters	Value
Time Iterator	120 :end time
pde:viscosity	0.01 0.02
wall bc	slip-friction slip no-slip
solver::equation residual tol	1.0e-6

5.3.1 Convergence analysis

For the fixed point iteration the stopping criterion is the Euclidean norm of the residual vector is less than 10^{-6} . We analyze the time dependent behaviour.

We take the time step (k) using the formula for CFL condition (2.8):

$$k = 0.15\frac{\text{hmin}}{\text{ubar}} \tag{5.1}$$

where ubar = 1 and hmin is the minimum cell size from the mesh, the constant value 0.15 is the Courant number small enough. We can change the time step by changing the value of the Courant number, CFL and small value of CFL is more suitable for the stability concern and for the convergence of fixed point iteration.

5.3.2 Sensitivity analysis

We study the effect of skin friction parameter to the reattachment point of recirculating vortex behind the step to learn about the sensitivity of the skin friction parameter used in the near wall modeling of turbulent boundary layer to the results.

To investigate the effect of the skin friction parameter of near wall modeling for turbulent boundary layer, the values of the skin friction parameter β are tested in the simulation where $\beta \in \{0.0, 0.001, 0.005, 0.01, 0.05, 0.1, 0.25, 0.5,$-$1.0, 5.0, 10.0, 100.0, 1000.0, 1.0e6\}$. The choice of β, $\beta \to 0$ prescribes perfect slip boundary conditions and $\beta \to \infty$ no slip boundary condition.

We do the computations for three different cases of boundary condition, given in table 5.2 named as wall bc. We compute the reattachment point of the recirculating vortex for viscosity parameters $\nu^{-1} = 50$ and $\nu^{-1} = 100$, given in table 5.2 named as pde:viscosity, and for the grid levels 3, 4 and 5, 5.1.

Parabolic inflow profile

The computations are performed for the parabolic inflow profile $\mathbf{u} = (u_1, u_2)^T$, with $u_1 = y(10 - y)/25$, $u_2 = 0$ on Γ_{infl} of the step channel.

slip-friction boundary condition

Streamlines of a two dimensional step channel are presented in Figure 5.3 for viscosity $\nu = 0.01$ and $\nu = 0.02$, for parabolic inflow and grid level 4.

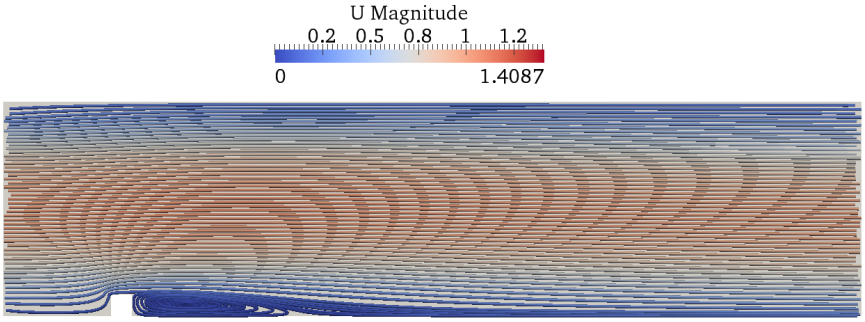

(a) Velocity Streamlines: for $\nu = 0.01$

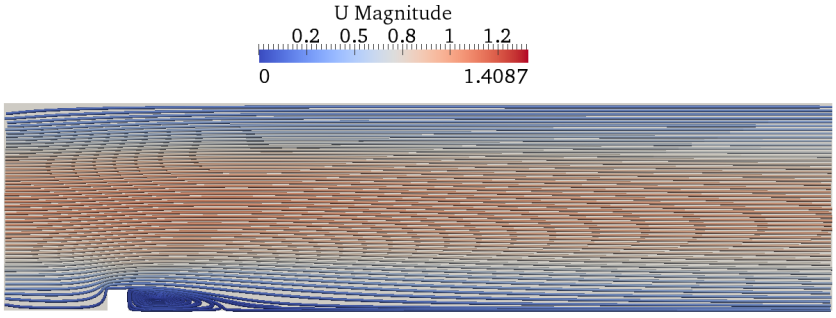

(b) Velocity Streamlines: for $\nu = 0.02$

Figure 5.3: Velocity Streamlines of flow in two dimensional channel with a step for $\beta = 0.1$, parabolic inflow

The plots in 5.4 and 5.5 show the tangential velocity for viscosity $\nu = 0.01$ and for parabolic inflow on the bottom wall in which the reattachment points can be pointed by the tangential velocity that is negative to the left of this reattachment point because of the recirculation of the vortex and positive to the right of that point.

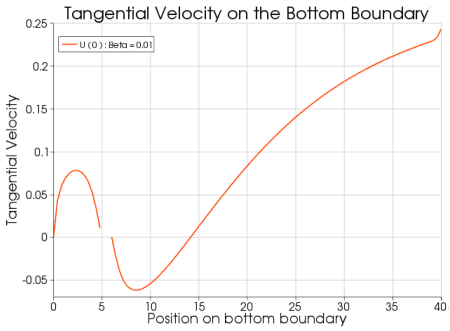

(a) Tangential Velocity: for $\beta = 0.01$

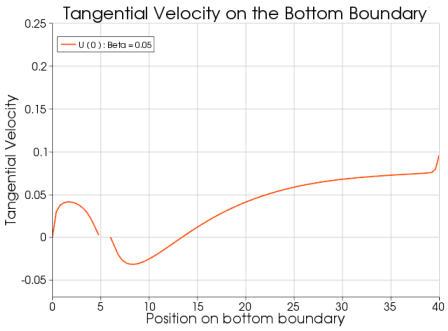

(b) Tangential Velocity: for $\beta = 0.05$

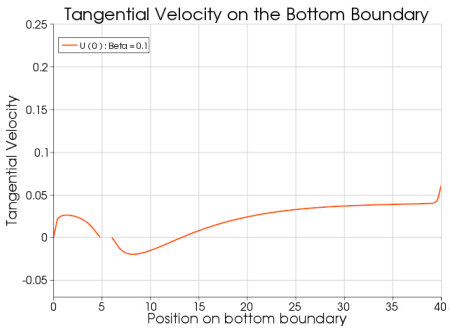

(c) Tangential Velocity: for $\beta = 0.1$

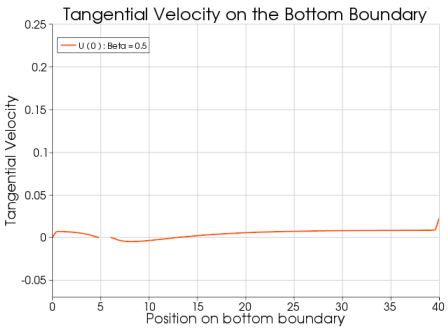

(d) Tangential Velocity: for $\beta = 0.5$

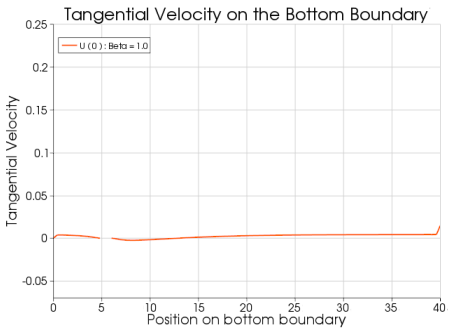

(e) Tangential Velocity: for $\beta = 1$

Figure 5.4: Tangential velocity at the bottom wall, for viscosity $\nu = 0.01$, for friction parameter $\beta = \{0.01, 0.05, 0.1, 0.5, 1.0\}$, for grid level 4, parabolic inflow

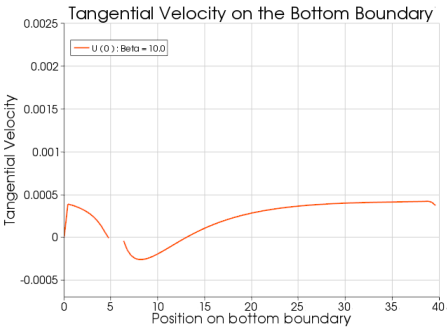

(a) Tangential Velocity: for $\beta = 10$

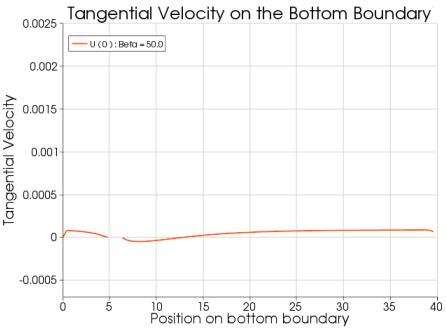

(b) Tangential Velocity: for $\beta = 50$

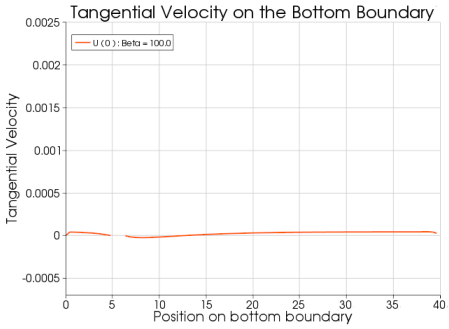

(c) Tangential Velocity: for $\beta = 100$

Figure 5.5: Tangential velocity at the bottom wall, for viscosity $\nu = 0.01$, for friction parameter $\beta = \{10.0, 50.0, 100.0\}$, for grid level 4, parabolic inflow

From the plots in 5.4 and 5.5 we observed that the tangential velocity decreases if the values of the skin friction parameter β increases.

The reattachment points for viscosity $\nu = 0.01$, for different skin friction parameters and for different grid levels are presented into the plots below 5.6 with the results from Volker John's numerical tests [12].

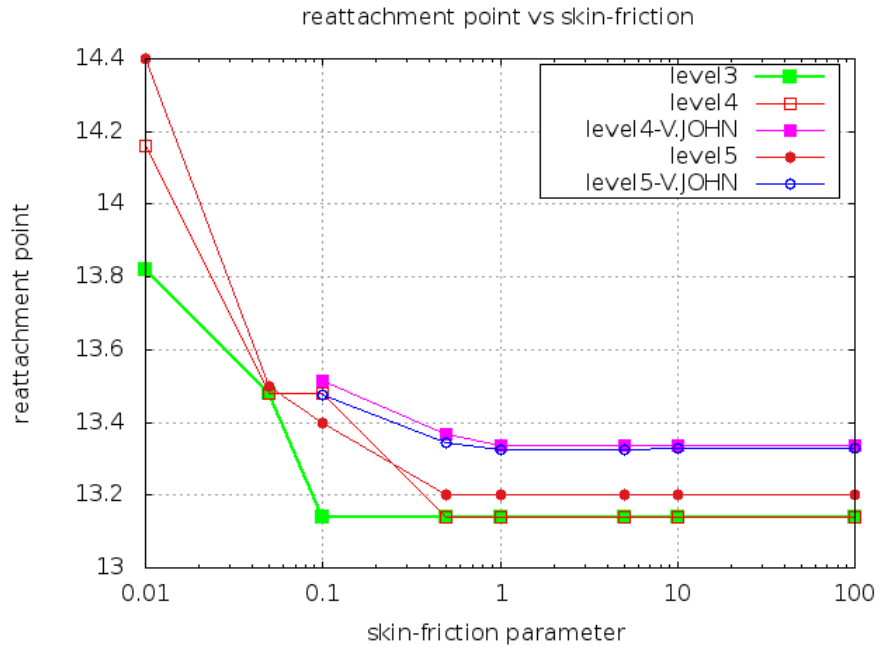

Figure 5.6: Reattachment point vs skin-friction of a two dimensional step channel, for viscosity $\nu = 0.01$, parabolic inflow

The plots in 5.7 and 5.8 show the tangential velocity for viscosity $\nu = 0.02$ on the bottom wall.

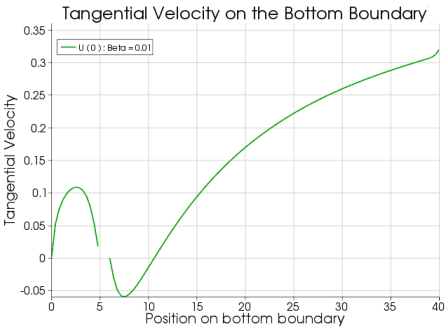

(a) Tangential Velocity: for $\beta = 0.01$

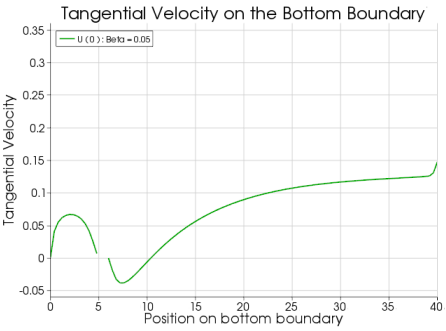

(b) Tangential Velocity: for $\beta = 0.05$

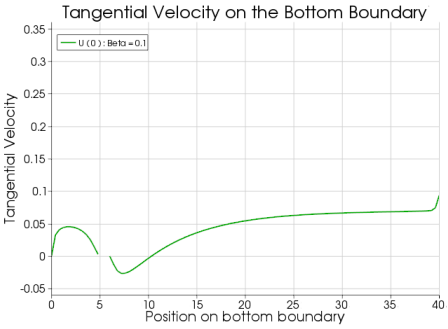

(c) Tangential Velocity: for $\beta = 0.1$

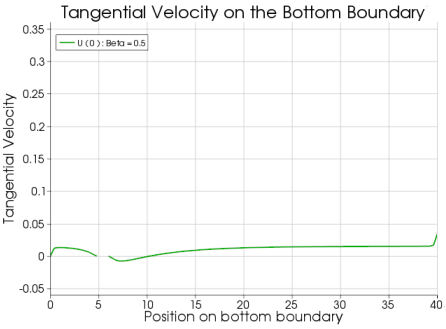

(d) Tangential Velocity: for $\beta = 0.5$

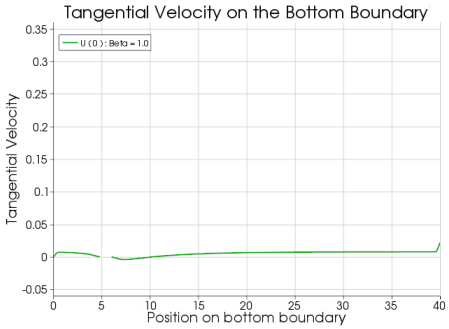

(e) Tangential Velocity: for $\beta = 1$

Figure 5.7: Tangential velocity at the bottom wall, for viscosity $\nu = 0.02$, for friction parameter $\beta = \{0.01, 0.05, 0.1, 0.5, 1.0\}$, for grid level 4, parabolic inflow

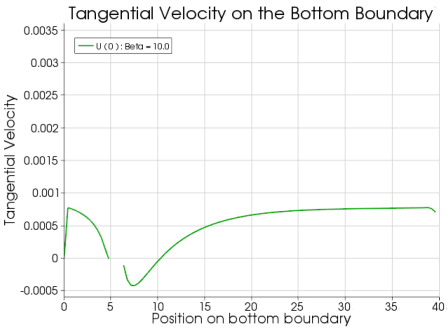

(a) Tangential Velocity: for $\beta = 10$

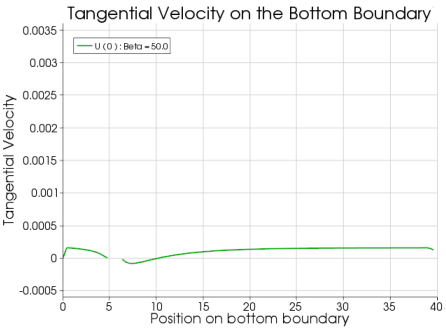

(b) Tangential Velocity: for $\beta = 50$

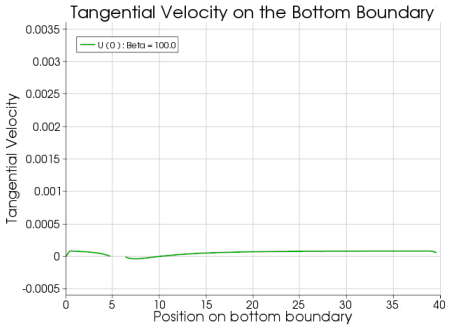

(c) Tangential Velocity: for $\beta = 100$

Figure 5.8: Tangential velocity at the bottom wall, for viscosity $\nu = 0.02$, for friction parameter $\beta = \{10.0, 50.0, 100.0\}$, for grid level 4, parabolic inflow

From the plots in 5.7 and 5.8 we observed that the tangential velocity decreases if we increase the value of skin friction parameter β.

The reattachment points for viscosity $\nu = 0.02$, for different skin friction parameters and for different grid levels are presented into the plots below 5.9 with the results from Volker John's numerical tests [12].

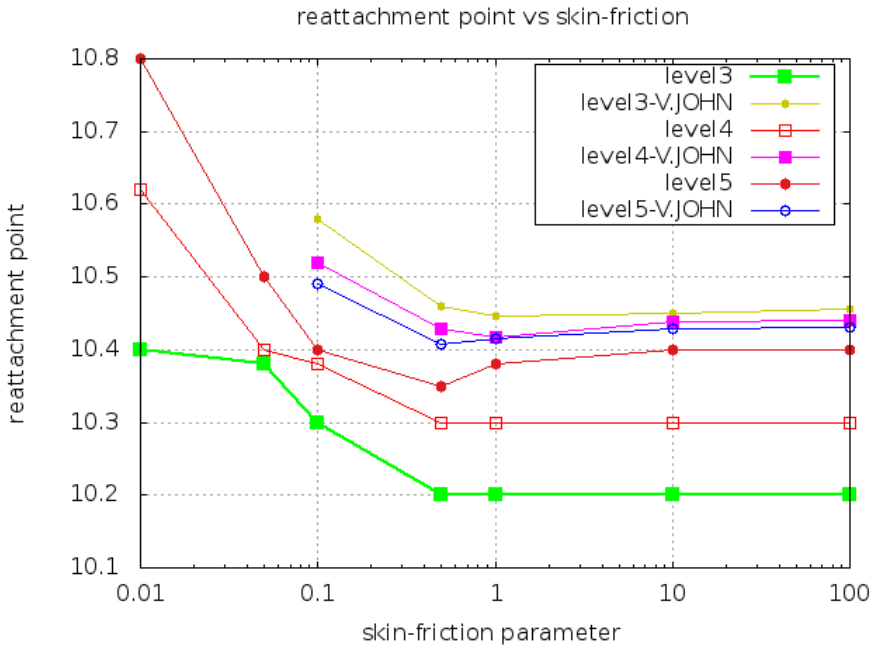

Figure 5.9: Reattachment point vs skin-friction of a two dimensional step channel, for viscosity $\nu = 0.02$, parabolic inflow

Perfect slip boundary condition

Tangential velocity for viscosity $\nu = 0.01$ and $\nu = 0.02$ using perfect slip boundary condition $\beta = 0$ is plotted, figure 5.10.

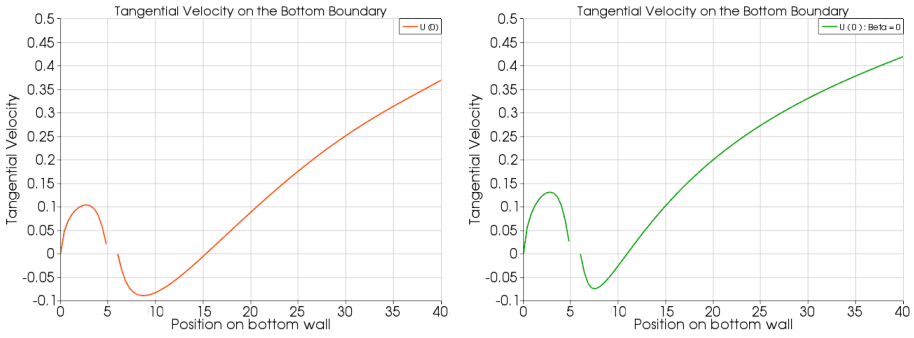

(a) Tangential Velocity: for $\beta = 0$

(b) Tangential Velocity: for $\beta = 0$

Figure 5.10: Tangential Velocity of a two dimensional step channel, for viscosity $\nu = 0.01$, and $\nu = 0.02$ parabolic inflow, perfect slip $\beta = 0$

No slip boundary condition

Streamlines of a two dimensional step channel are presented in Figure 5.11 for viscosity $\nu = 0.01$ and $\nu = 0.02$, for parabolic inflow using no slip boundary condition.

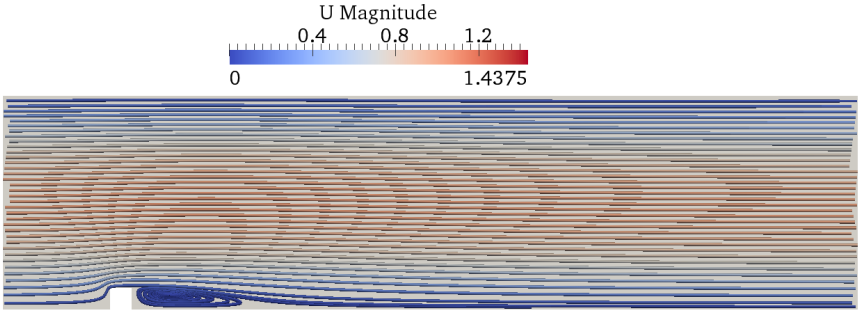

(a) Velocity Streamlines: for no-slip

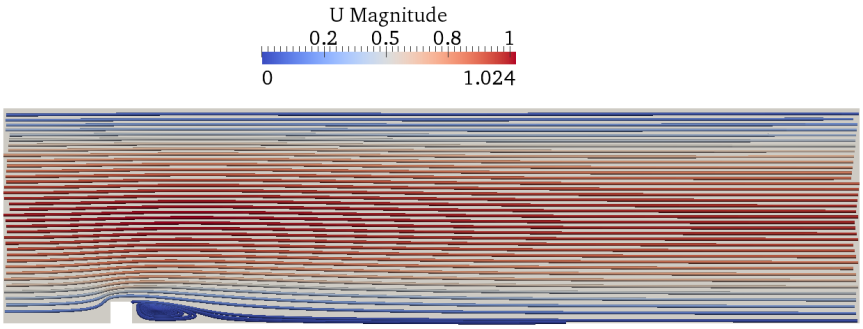

(b) Velocity Streamlines: for no-slip

Figure 5.11: Velocity Streamlines of flow in two dimensional channel with a step for no slip boundary condition, for parabolic inflow

Tangential velocity for viscosity $\nu = 0.01$ and $\nu = 0.02$ using no slip boundary condition is plotted, figure 5.12.

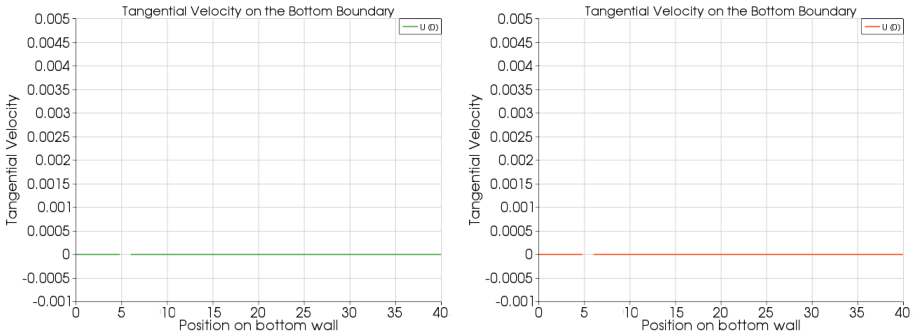

(a) Tangential Velocity: for no-slip

(b) Tangential Velocity: for no-slip

Figure 5.12: Tangential Velocity of a two dimensional step channel, for viscosity $\nu = 0.01$, and $\nu = 0.02$ parabolic inflow, no slip boundary condition

From figure 5.12, we see that the tangential velocities along the bottom wall of the step channel are zero for the no slip boundary condition.

Remarks

From the figure 5.6 and 5.9 we observe that, the reattachment length of the recirculating vortex of $\nu^{-1} = 50$ is smaller than that of $\nu^{-1} = 100$.

For both $\nu^{-1} = 100$ and $\nu^{-1} = 50$, the reattachment length of the recirculating vortex behind the step increases *i.e.* the position of the reattachment point moves towards the outflow boundary when the skin friction parameter $\beta \in \{0.0, 0.01, 0.05, 0.1, 0.5\}$ decreases on the boundary and the position of reattachment point remains same and close to the step if the skin friction parameter, $\beta \in \{0.5, 1.0, 10.0, 100\}$.

But for grid level 5 and for $\nu^{-1} = 50$, the position of the reattachment point for $\beta \in \{0.5, 1.0, 10.0, 100.0\}$ comes closer towards the step with β decreasing and from a certain value of β if we increase β, the position of a reattachment point remains same. But for $\beta \in \{0.0, 0.01, 0.05, 0.1, 0.5\}$, the position of the reattachment point moves towards the outflow boundary with β decreasing. So for a certain value of β, we get a local minimum of the positions of the reattachment point.

From Figure 5.6 and 5.9, comparing our results with the results of Volker John numerical tests [12], we observed that the positions of the reattachment points for different values of skin friction parameter is smaller than the results of Volker John, since we have used G2 turbulent simulation technique as our numerical scheme and this scheme uses streamline diffusion for numerical stabilization, so the technique is more diffusive.

It is also observed from the figure that, the values of the stabilizing parameter of finer grid level are smaller than that of the coarser level, so the position of the reattachment point for finer grid level is higher than that of coarser level as the numerical scheme is less diffusive.

From figure 5.4, 5.5 and 5.7, 5.8 we observed that the tangential velocity decreases if the values of the skin friction parameter β increases and for the very high values of β the tangential velocity tends to zero which behaves like a no slip boundary condition.

From figure 5.10 it is seen that the tangential velocity of using the perfect slip boundary condition is bigger than the tangential velocity of using slip with friction boundary condition and also we get the bigger reattachment length.

Constant inflow profile

Results for computations are presented when constant inflow profile $u_1 = 1, u_2 = 0$ is used on the inlet.

Slip friction boundary condition

Streamlines of a two dimensional step channel for constant inflow are presented in Figure 5.13 for viscosity $\nu = 0.01$, $\nu = 0.02$ and for grid level 4.

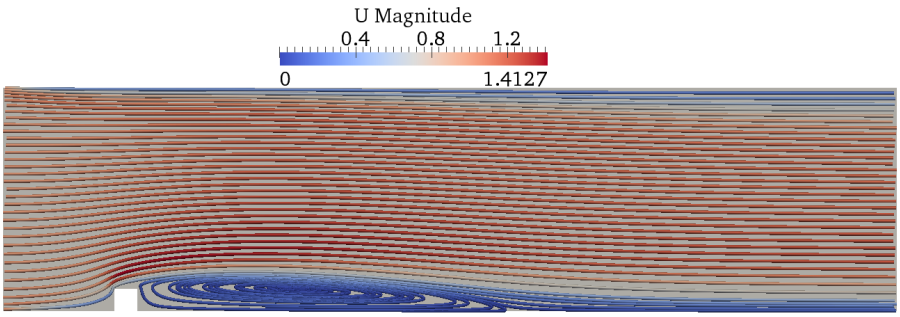

(a) Velocity Streamlines: for $\nu = 0.01$

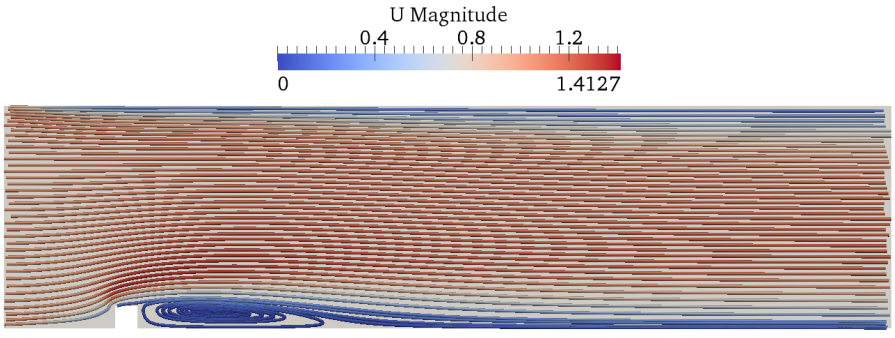

(b) Velocity Streamlines: for $\nu = 0.02$

Figure 5.13: Velocity Streamlines of flow in two dimensional channel with a step for $\beta = 0.1$ and constant inflow

The plots in 5.14 and 5.15 show the tangential velocity on the bottom wall for viscosity $\nu = 0.01$.

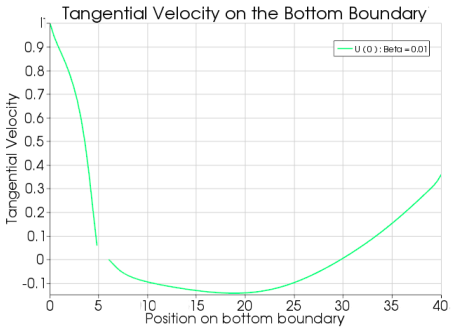

(a) Tangential Velocity: for $\beta = 0.01$

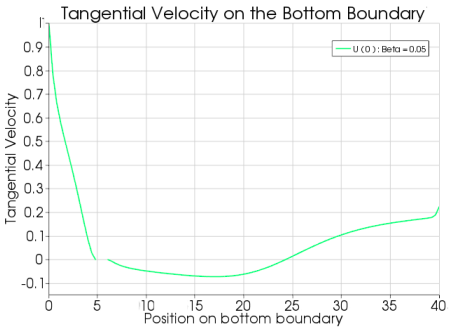

(b) Tangential Velocity: for $\beta = 0.05$

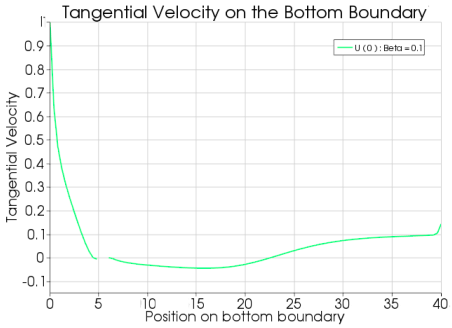

(c) Tangential Velocity: for $\beta = 0.1$

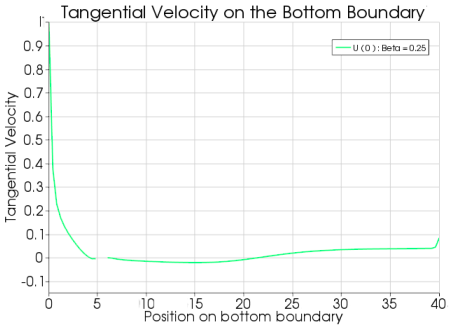

(d) Tangential Velocity: for $\beta = 0.25$

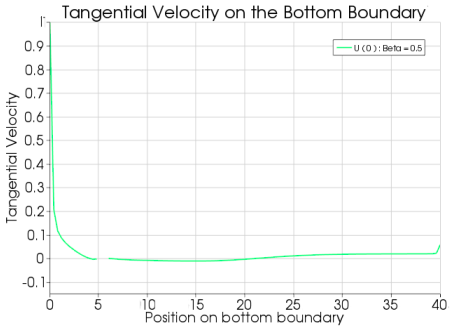

(e) Tangential Velocity: for $\beta = 0.5$

Figure 5.14: Tangential velocity at the bottom wall, for viscosity $\nu = 0.01$, for friction parameter $\beta = \{0.01, 0.05, 0.1, 0.25, 0.5\}$, for grid level 4 and constant inflow

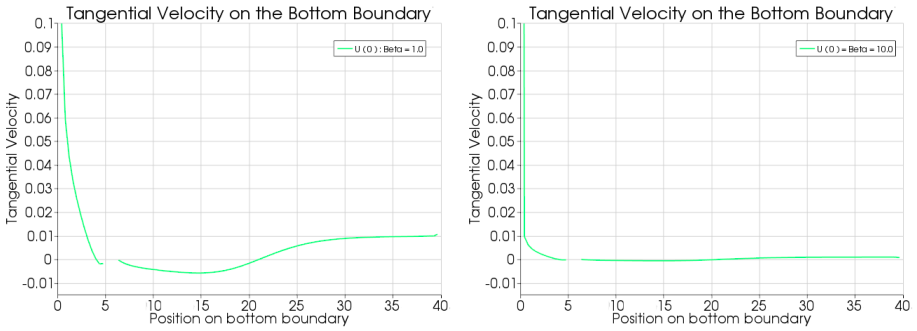

(a) Tangential Velocity: for $\beta = 1$ (b) Tangential Velocity: for $\beta = 10$

Figure 5.15: Tangential velocity at the bottom wall, for viscosity $\nu = 0.01$, for friction parameter $\beta = \{1.0, 10.0\}$, for grid level 4 and constant inflow

The plots in 5.14 and 5.15 shows that tangential velocity along the bottom wall decreases if the values of the skin friction parameter increases.

Positions of reattachment points for viscosity $\nu = 0.01$, for different values of skin friction parameters and for different grid levels are presented into the figures below 5.16 also the results of the numerical tests from Volker John [12].

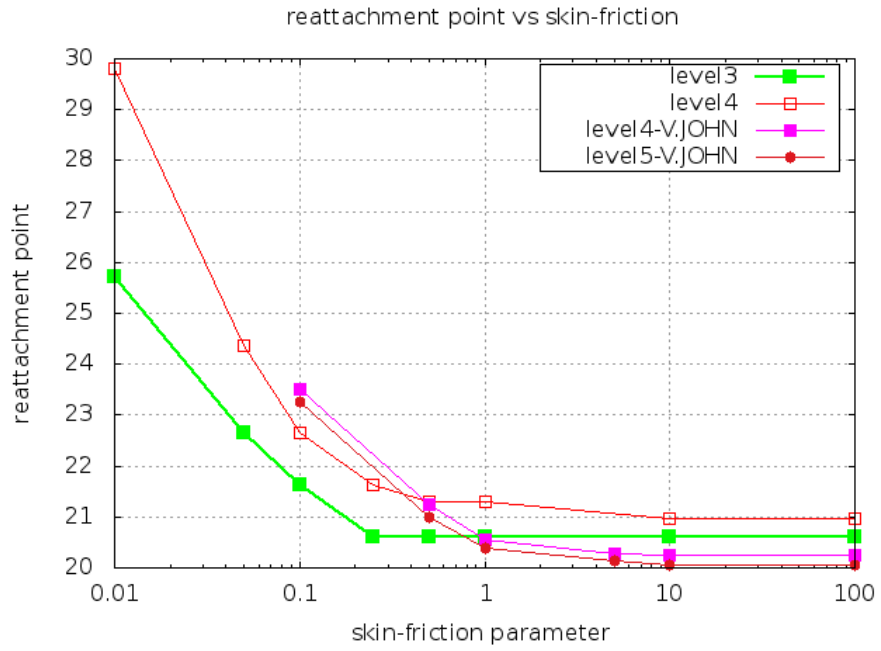

Figure 5.16: Reattachment point vs skin-friction of a two dimensional step channel, for viscosity $\nu = 0.01$, constant inflow

Tangential velocities for viscosity $\nu = 0.02$ are presented into the figures 5.17 and 5.18.

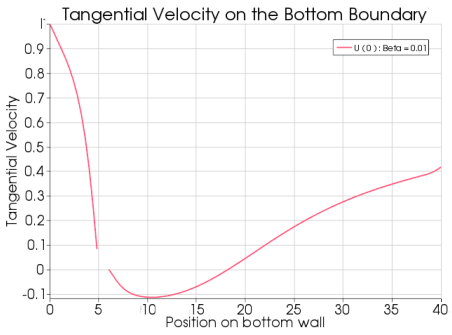

(a) Tangential Velocity: for $\beta = 0.01$

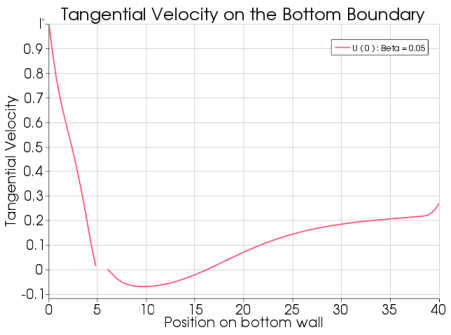

(b) Tangential Velocity: for $\beta = 0.05$

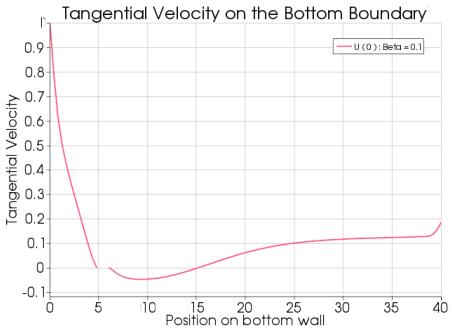

(c) Tangential Velocity: for $\beta = 0.1$

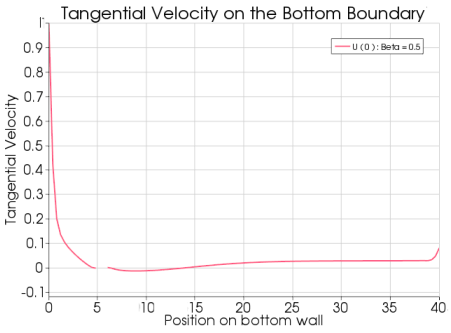

(d) Tangential Velocity: for $\beta = 0.5$

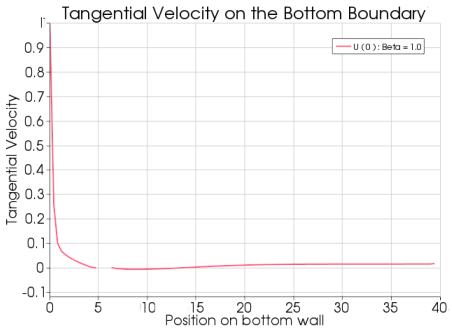

(e) Tangential Velocity: for $\beta = 1$

Figure 5.17: Tangential velocity at the bottom wall, for viscosity $\nu = 0.02$, for friction parameter $\beta = \{0.01, 0.05, 0.1, 0.5, 1.0\}$, for grid level 3 and constant inflow

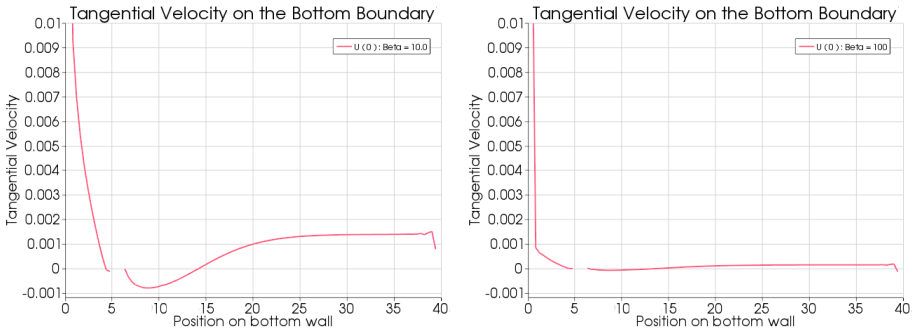

(a) Tangential Velocity: for $\beta = 10$ (b) Tangential Velocity: for $\beta = 100$

Figure 5.18: Tangential velocity at the bottom wall, for viscosity $\nu = 0.02$, for friction parameter $\beta = \{10.0, 100.0\}$, for grid level 3 and constant inflow

From the figures 5.17 and 5.18 it is observed that the tangential velocities decreases if the values of skin friction parameter increases.

The positions of the reattachment points for viscosity $\nu = 0.02$, for different values of skin friction parameters and for different grid levels from our computation and from Volker John's [12] are presented into the figure 5.19.

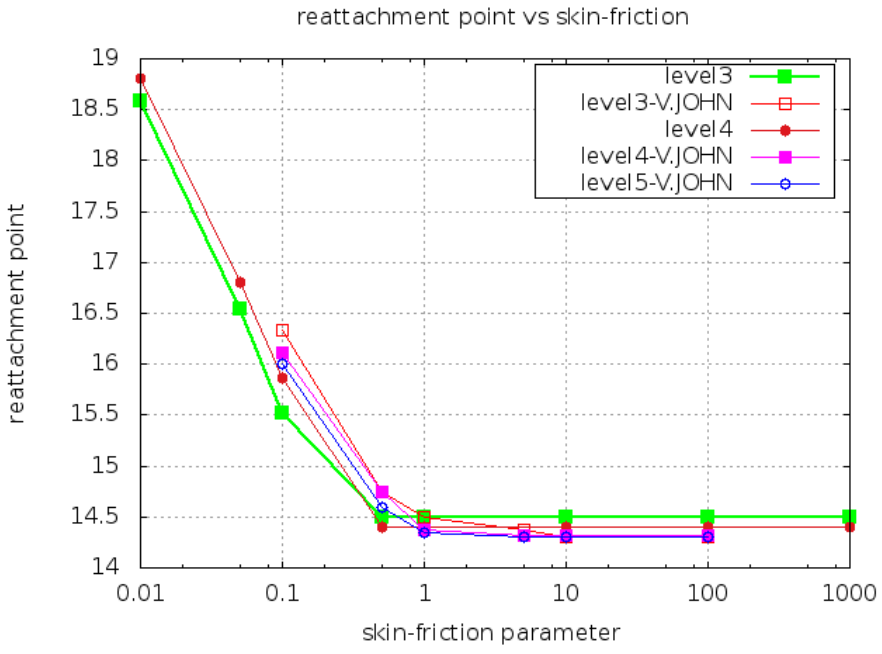

Figure 5.19: Reattachment point vs skin-friction of a two dimensional step channel, for viscosity $\nu = 0.02$ and constant inflow

Perfect slip boundary condition

Tangential velocity for viscosity $\nu = 0.01$ and $\nu = 0.02$ using perfect slip boundary condition:

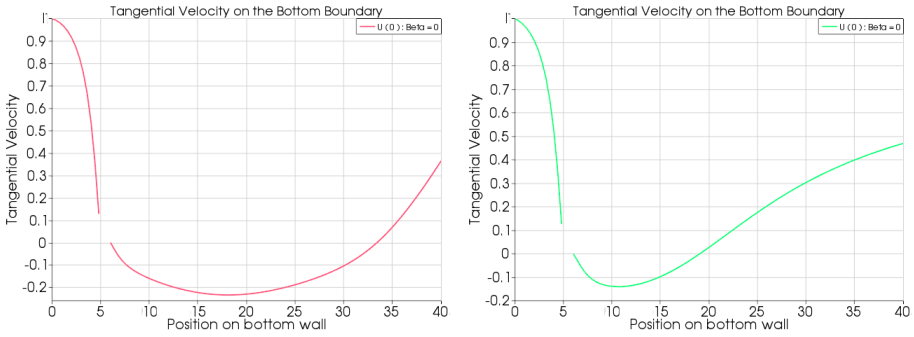

(a) Tangential Velocity: for $\beta = 0$ (b) Tangential Velocity: for $\beta = 0$

Figure 5.20: Tangential Velocity of a two dimensional step channel, for viscosity $\nu = 0.01$, and $\nu = 0.02$ constant inflow, perfect slip $\beta = 0$

No slip boundary condition

Streamlines of a two dimensional step channel are presented in Figure 5.21 for viscosity $\nu = 0.01$ and $\nu = 0.02$, for constant inflow using no slip boundary condition.

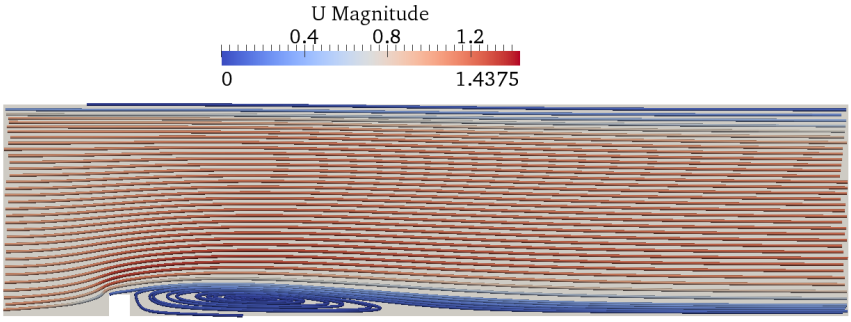

(a) Velocity Streamlines: for no-slip

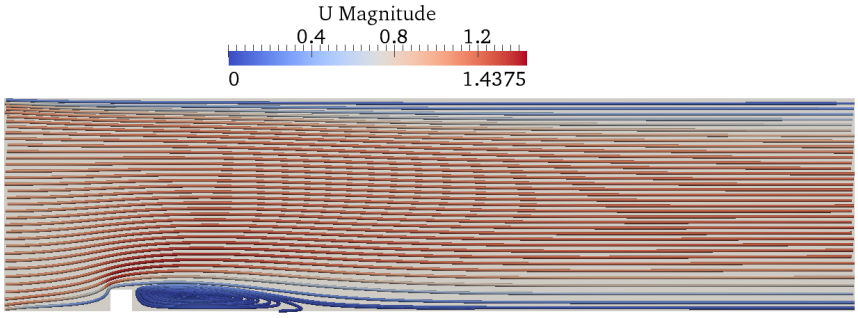

(b) Velocity Streamlines: for no-slip

Figure 5.21: Velocity Streamlines of flow in two dimensional channel with a step for no slip boundary condition and for constant inflow

Tangential velocity for viscosity $\nu = 0.01$ and $\nu = 0.02$ using no-slip boundary condition for constant inflow:

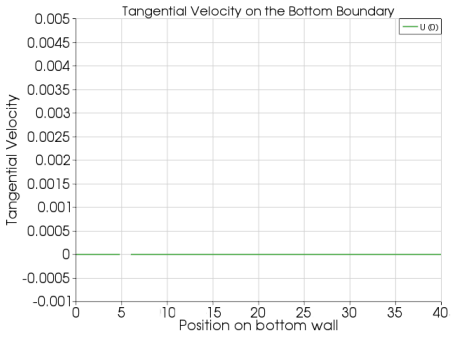

(a) Tangential Velocity: for no-slip

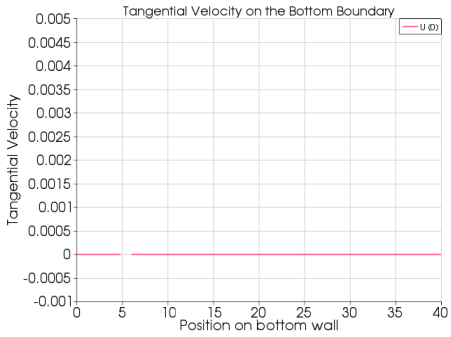

(b) Tangential Velocity: for no-slip

Figure 5.22: Tangential Velocity of a two dimensional step channel, for viscosity $\nu = 0.01$, and $\nu = 0.02$ constant inflow, no-slip boundary condition

Remarks

From figure 5.16 and 5.19, for viscosity $\nu^{-1} = 50$ and for viscosity $\nu^{-1} = 100$ for grid level 3, we get the position of the reattachment point moves in the direction of outflow boundary if we decrease the value of skin friction parameter $\beta \in \{0.0, 0.01, 0.05, 0.1, 0.5\}$ and the position of reattachment point remains same and close to the step if the skin friction parameter, $\beta \in \{0.5, 1.0, 10.0,$-$100\}$.

For viscosity $\nu^{-1} = 100$ for grid level 4, the position of the reattachment point moves towards the outflow boundary for smaller values of skin friction parameter.

And the reattachment length of the recirculating vortex of $\nu^{-1} = 50$ is smaller than that of $\nu^{-1} = 100$.

From figure 5.16 and 5.19, comparing our results with the results of Volker John numerical tests [12], it is observed that for smaller values of β, our simulation results smaller values of positions of reattachment point because of stabilized numerical scheme.

From 5.14, 5.15 and 5.17, 5.18 we get the tangential velocities decrease if the values of the skin friction parameter increases and also for very high values of β the tangential velocity tends to zero, behaves like a no slip boundary condition.

From figure 5.20 it is seen that, the tangential velocity of using the perfect slip boundary condition is bigger than the tangential velocity of using slip with friction boundary condition and also we get the bigger reattachment length.

5.3.3 Concluding Remarks

It is observed that using Wall shear stress modeling of turbulent boundary layer the position of the reattachment point for large values of skin friction parameter β is very close to the position if we use no slip boundary condition on the top and bottom wall on a fine grid level.

5.4 Sensitivity Analysis of Wall Model

We analyzed the effect of the skin friction parameter of the boundary wall model of turbulent boundary layer i.e. Wall Shear Stress model to the results of interest. Also studied no slip boundary condition and perfect slip boundary condition into the simulations. We observed that using wall model into the simulation is more precised and capable to represent the characteristic flow features.

5.5 Concluding remarks

For the Large eddy simulation to characterize the small scale features there is great importance of how well we can treat the boundary layer. To treat the turbulent boundary wall we used Wall Shear stress model and we analyzed the effect of the friction parameter of that model to the results of interest with

different boundary conditions. We observed that this wall boundary model is able to characterize the turbulent flow features.

Chapter 6

Case Study II : Flow Around a circular cylinder

A numerical study for flow past a circular cylinder using the wall shear stress model 3, is presented. To understand the different properties of the turbulent flows and to characterize the effect of the near-wall turbulence modeling in the simulation, we analyze the separation of turbulent flows which is a significant flow phenomena for turbulent flows and to predict these phenomena with accuracy is challenging.

A simple wall model, wall shear stress model, is used to model the effect of the boundary layer, based on a slip with friction boundary condition. The idea is that the main effect of the boundary layer on the flow is skin friction.

6.1 Test Problem

To investigate the accuracy and viability of large eddy simulation, wall modeling into the simulation technique has important role. It is significant to have the study of the wall modeling in well defined test problems. We take the test problem flow past a circular cylinder from Turek's test case [24]. We investigate the sensitivity of the model parameters of wall modeling.

6.1.1 Motivation of the Test Problem

Flow past a circular cylinder with its complex features, represents a canonical problem for validating new approaches in computation of fluid dynamics. Also, the cylinder is known for its drag crisis, which reflects the great difference in separation between laminar and turbulent boundary layers.

As the Reynolds number increases, different regions of the flow past a circular cylinder undergo transition to turbulence; the wake, shear layers and finally boundary layers, causing a delayed separation and so called drag crisis. Although limited, there are some experimental results available, from which conclusions can be drawn about the flow with the computational results.

6.1.2 Application of the Test Problem

The flow past vehicles and airplane components such as landing gear causes massive three dimensional separation. So the study of the test problem, flows around a circular cylinder which also causes massive separation at high Reynolds number, is very important to observe the accuracy of the simulation technique that we can apply to the real engineering problems to get the engineering accuracy.

6.2 Flow around a Circular Cylinder

For any section of the cylinder, an angle θ starting from the upstream stagnation point can be defined. From the upstream stagnation point, where the pressure is very high, the flow accelerates and the pressure near the boundary is decreasing up to $\theta \approx 90^0$, where the pressure starts to increase again which results in an adverse pressure gradient acting as a negative force in the momentum equation. If the momentum close to the boundary is too low, the adverse pressure gradient force the flow to separate. Computer simulation of subcritical Reynolds number flow past a circular cylinder is today a routine, e.g. with LES, where laminar boundary layers are modeled by no slip velocity boundary conditions. On the other hand supercritical flow with turbulent boundary layers poses great challenges with respect to the modeling of turbulent boundary layers, which are too expensive to resolve for very high Re.

Wall shear stress model is used, where the local shear stress at the solid wall is assumed to be proportional to the wall tangential velocity, similar to the model by Schumann [23]. The choice of proper parameters depends on the computational mesh, the solution itself and problem data. The aim is not to determine the optimal parameters of the model for a certain Re, but instead to study the computed solutions for a range of such model parameters.

6.3 Two dimensional Flow around a Circular Cylinder

Geometry Specifications

The geometry of the domain of a two dimensional circular cylinder in our computation is taken from [24], presented in Figure 6.1.

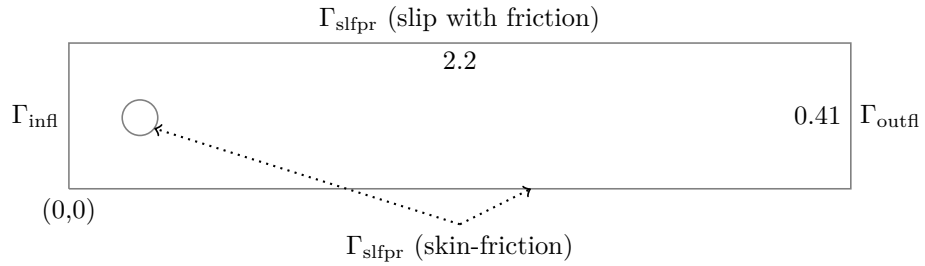

Figure 6.1: Geometry for two dimensional circular cylinder

An inflow boundary condition specified on the left boundary Γ_{infl} of the domain, an outflow boundary condition Γ_{outfl} where the flow leaves on the right boundary of the domain, a slip with friction boundary condition on the top and on the bottom boundary of the domain and around the circular cylinder of radius 0.05 centered at $(0.2, 0.2)$ are prescribed in Figure 6.1.

To analyze the sensitivity of the wall model different boundary conditions are prescribed as different test case on the boundary Γ_{slfpr} : perfect slip boundary condition and slip with skin friction boundary condition. The results for a constant inflow profile as the inflow boundary condition are analyzed.

Mesh Generation

We performed our simulations with the unstructured grid presented in Figure A.1d. The degrees of freedom for finer level is 2×20739 for computing the velocity and pressure.

Model Parameters

The details of the computational parameters are summarized in Table 6.1 and the meaning of the parameters are discussed in 5.3. We take wall boundary condition as a model parameter where wall boundary conditions are defined into our wall shear stress model.

Table 6.1: Computational parameters used in the simulation

Parameters	Value
Time Iterator	2.2 :end time
pde:viscosity	0.05
wall bc	slip-friction slip
solver::equation residual tol	1.0e-6

6.3.1 Convergence Analysis

For the fixed point iteration the stopping criterion is the Euclidean norm of the residual vector is less than 10^{-6} . We analyze the time dependent behaviour.

We take the time step (k) using the formula for CFL condition (2.8):

$$k = 0.0015\frac{\text{hmin}}{\text{ubar}} \tag{6.1}$$

where ubar = 1 and hmin is the minimum cell size from the mesh, the constant value 0.0015, the courant number is chosen very small, where we can change the time step by changing this constant value and small constant value is more suitable for the stability concern and for the convergence of fixed point iteration.

6.3.2 Sensitivity Analysis

We study the effect of skin friction parameter to the velocity profiles along the center line to learn about sensitivity of the skin friction parameter to the results. We run the simulation for different values of β and for the constant inflow profile, $u_1 = 1$, $u_2 = 0$ at the inlet boundary.

The velocity profiles and pressure for flow around a circular cylinder in 2D are presented in figures 6.2, 6.3.

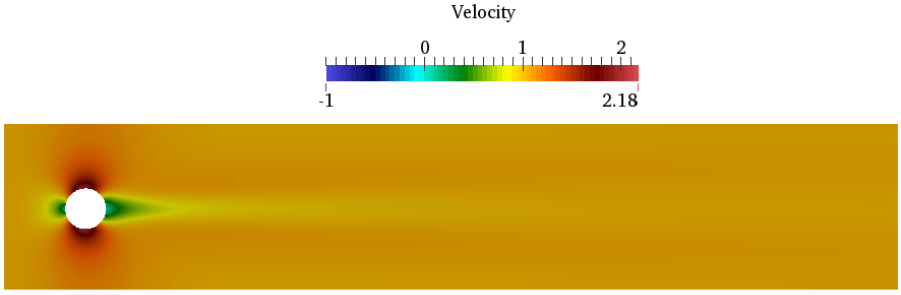

(a) Velocity profile: $\beta = 0$

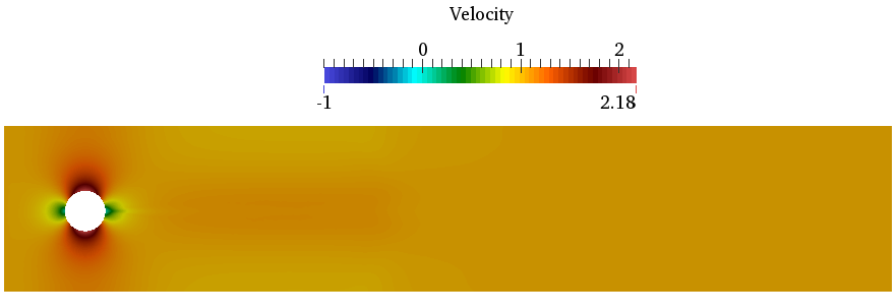

(b) Velocity profile: $\beta = 0.001$

Figure 6.2: Velocity Profiles for flow around a circular cylinder for constant inflow: for different β

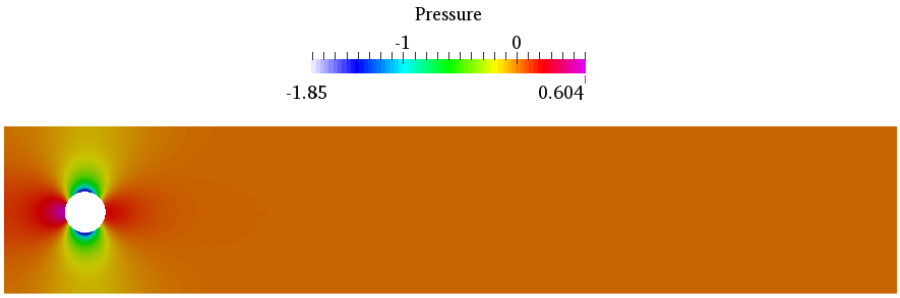

(a) Pressure: $\beta = 0$

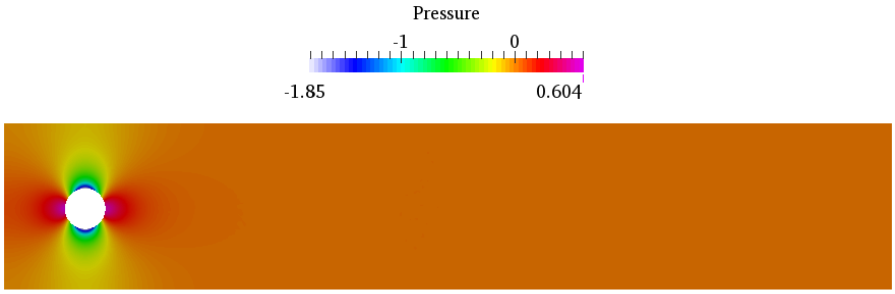

(b) Pressure: $\beta = 0.001$

Figure 6.3: Pressure for flow around a circular cylinder for constant inflow: for different β

The following figure represent the velocity along the centerline of the circular cylinder.

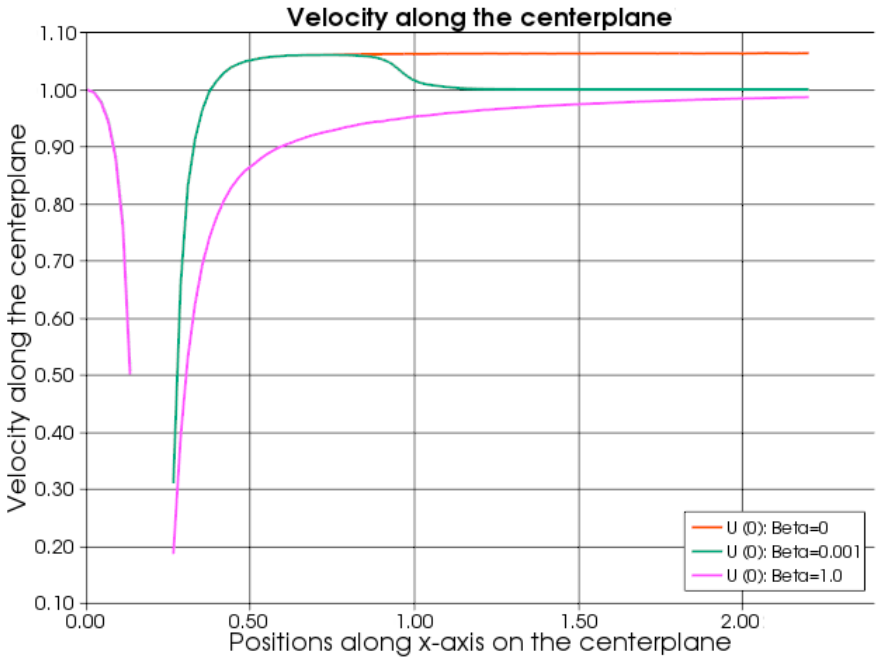

Figure 6.4: Velocity along the centerline for flow around a circular cylinder: for different values of β

6.3.3 Remarks

For flow around a circular cylinder, the recovery of the velocity behind the circular cylinder along the centerline is very strong.

6.4 Sensitivity study with respect to skin friction

The flow past the circular cylinder is computed using the wall shear stress model in G2 turbulence simulation technique for different values of β, to determine the sensitivity of the solution with respect to β. If we decrease the skin friction parameter for a low Reynolds number flow, we observed a faster and stronger recovery of the velocity along the centerline behind the circular cylinder.

6.5 Concluding Remarks

Numerical studies shows that the flow behavior for flow around a circular cylinder for different values of skin friction parameter of wall shear stress model is different. So with the parametric study of wall shear stress model we analyzed the sensitivity of near wall turbulence modeling.

Chapter 7

Comparison of Numerical Results with Experimental Results

For the experimental validation of near-wall turbulence modeling in G2 turbulence Simulation Technique, a comparison of numerical results with the experimental results is performed and to compare our results, established experimental databases are used, available in different published works. In this project, we focused on Wall shear stress model as a near-wall turbulence modeling for G2 Turbulence Simulation Technique, So we presented the results for different skin friction parameters to compare our results with the available experimental results.

7.1 Test Problems

We have chosen the test cases for which the flows have high Reynolds numbers and the geometry is complex where the significant features are recirculation length or point of separation and also the experimental results are available to compare with the numerical simulations. Flow around a surface mounted cube and flow around a square cylinder are two test cases, for which we run the simulations and compare the reattachment length for different skin friction parameters to compare with the experimental results.

7.1.1 Flow Around a Surface Mounted Cube

Flow around a surface mounted cube is chosen as a test problem for which the experimental results are available. For this test problem experimental results are available, published by Martinuzzi and Tropea [20] and Hussain and Martinuzzi [8]. There are also some numerical results available carried out by Large Eddy Simulations, show high degree of accuracy [13] and also a RANS approach with the $v^2 - f$ turbulence model [5] shows a good agreement with the experimental data.

7.1.2 Flow Around a Square Cylinder

For the test problem flow around a square cylinder, experimental data is available from the work of Lyn et al. [33]. Also some numerical results are available show good agreement with the experimental data [13].

7.2 Test Case I: Flow around a Surface Mounted Cube

We considered flow around a surface mounted cube into a channel as a test problem. The geometry and the flow conditions of the test case are taken similar to the experimental test problem from [5, 8].

Geometry Specifications

The geometry of the domain of a surface mounted cube flow used in the computation is presented in the Fig. 7.1, and this specification is taken from [5].

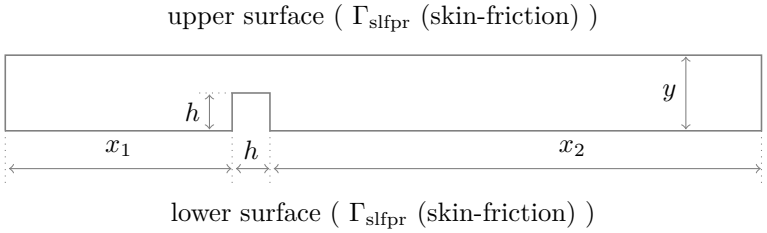

Figure 7.1: Geometry for flow over a surface mounted cube in 2D

In the figure 7.1, x is the length of the channel, y is the height of the channel and h is the height of the cube. The details of the computational domain for the surface mounted cube flow is presented in the table 7.1.

Table 7.1: Computational domain for the surface mounted cube flow

x_1/h	x_2/h	y/h
6	13	2

An inflow boundary condition specified on the left boundary of the domain, an outflow boundary condition where the flow leaves on the right boundary of the domain, a slip with friction boundary condition on the top and bottom boundary with the step of the domain are prescribed. For fully developed flow, the cube is located at a distance $6h$ from the inlet boundary. The simulations are run for the constant inflow at the inlet.

Mesh Generation

We performed the simulations with the initial grid (level 0) presented in figure 7.2. Initially, for the grid level 0, the horizontal grid lines are set at $y \in \{0.2, 0.4, 0.6, 0.8, 1, 1.2, 1.4, 1.6\}$ and the vertical grids are at $x \in \{2, 4, 4.5, 5, 5.2, 5.4, 5.6, 5.8, 6, 7, 7.2, 7.4, 7.6, 7.8, 8, 8.5, 9, 10, 12, 14, 16, 18\}$.

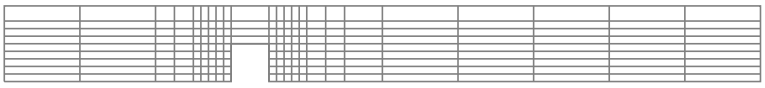

Figure 7.2: Computational grid (level 0) for surface mounted cube in 2D

Then we generate the higher level computational grids for the numerical studies using dolphin mesh generator presented in the Table 7.2.

Table 7.2: Degrees of freedom for the surface mounted cube in 2D

Level	Total
0	480
3	26450

Model Parameters

Details of the computational parameters are summarized in Table 7.3.

Table 7.3: Computational parameters for surface mounted cube simulations

Parameters	Value
Time Iterator	20 :end time
pde:viscosity	2.5e-5
wall bc	slip-friction
solver::equation residual tol	1.0e-6

7.2.1 Comparison of Numerical and Experimental Results

Concerning the time stability, for the time stepping we have chosen the Courant–Friedrichs–Lewy number 0.15:

$$k = \mathrm{CFL}\frac{\mathrm{hmin}}{\mathrm{ubar}} \tag{7.1}$$

where ubar = 1, hmin is the minimum cell size from the mesh and CFL is the Courant–Friedrichs–Lewy number.

The simulations are performed for the values of the skin friction parameter β where $\beta \in \{0.001, 0.01, 0.1, 0.5, 1.0\}$ for slip-friction boundary condition.

The Reynolds number is taken $Re = 4e4$ based on the velocity at the inlet and height of the cube, $Re = \frac{uh}{\nu}$, to compare our results with experimental results. We compute the reattachment length of the recirculating vortex for viscosity parameter $\nu = 2.5e-5$, given in table 7.3 named as pde:viscosity, and for the grid level 3, 7.2. Results for computations are presented when constant inflow profile $u_1 = 1, u_2 = 0$ is used at the inlet.

The velocity streamlines for flow over a surface mounted cube in 2D are presented in figure 7.3.

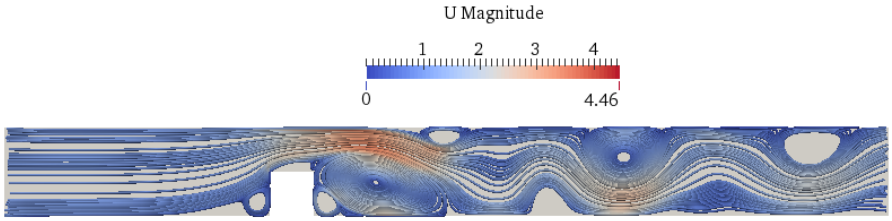

Figure 7.3: Velocity Streamlines for flow over a surface mounted cube in 2D : Numerical Results

The following figures represent the tangential velocity along the surface in two dimension for time $t = 20s$.

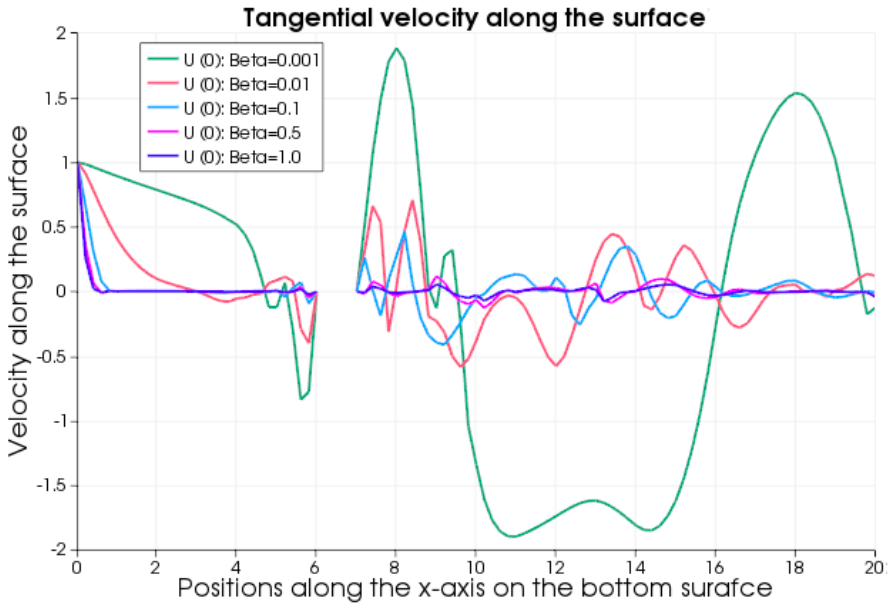

Figure 7.4: Tangential velocity at the bottom wall for different β

Table 7.4: Reattachment length for flow around a surface mounted cube in 2D (Both Experimental and Computational results)

Works performed By	Model	Skin-friction (β)	Reattachment Length
Martinuzzi and Tropea [20]	Experimental	-	1.62
Our Studies	G2 Simulation with Wall Stress Model	$\beta = 0.001$	2.2
		$\beta = 0.01$	1.0
		$\beta = 0.1$	1.0
		$\beta = 0.5$	1.6
		$\beta = 1.0$	1.6

We compute the length of the reattachment length, and observed that the value of skin friction parameter is not certain for which the numerical result will be in a good match with the experimental results.

7.2.2 Remarks

The flow around a surface mounted cube is a three dimensional obstacle, so the streamwise vortices is generated within the shear layer. For these vortices the recirculation region is reorganized and also the downstream recovery region is influenced [20] so the recirculation length in three dimension would be different than the results in two dimension.

7.3 Test Case II: Flow around a Square Cylinder

The geometry and flow conditions of this test problem are taken similar to the experimental data from [33, 5].

Geometry Specifications

The geometry of the domain for flow around a square cylinder in 2D used in this computation is presented in the figure 7.5.

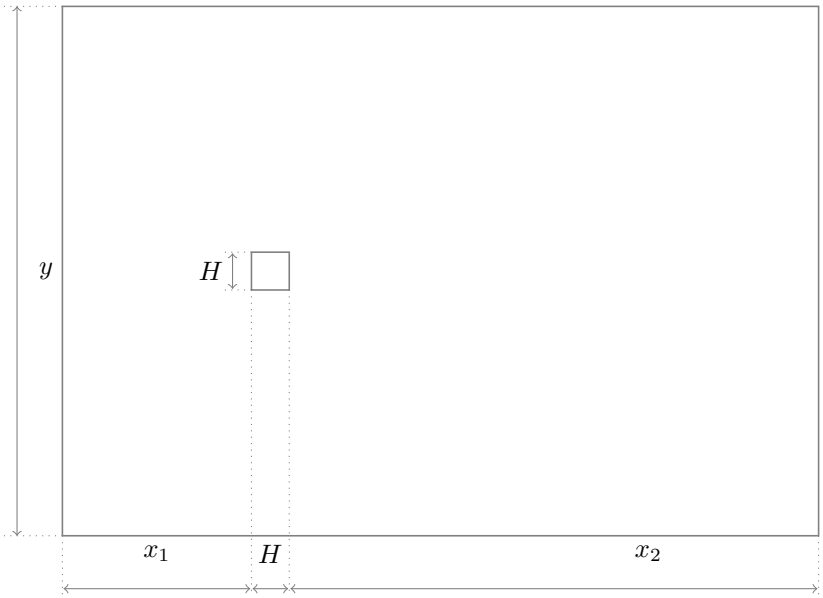

Figure 7.5: Geometry for flow around a square cylinder in 2D

On the left boundary of the domain an inflow boundary condition and on the right boundary of the domain an outflow boundary condition are specified. On the top and bottom boundary of the domain and around the square cylinder inside the domain a slip with friction boundary condition is prescribed. The simulations are run for the constant inflow at the inlet.

Mesh Generation

The initial grid (level 0) for the simulations is presented in the figure 7.6.

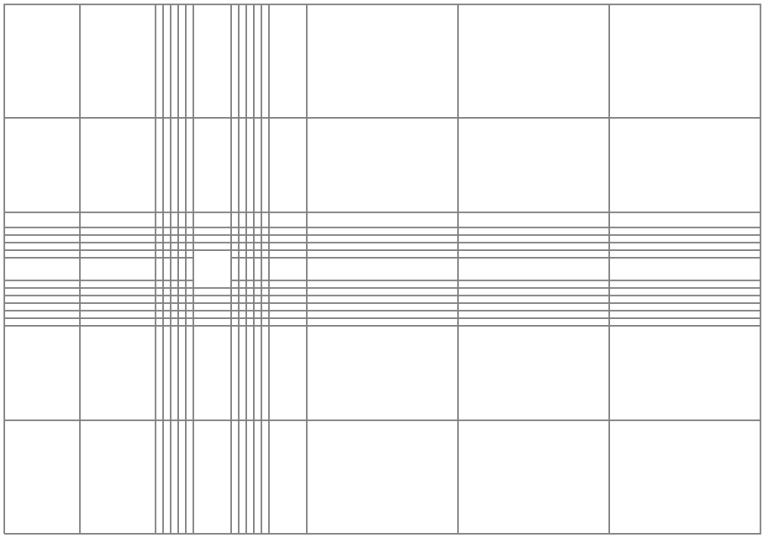

Figure 7.6: Computational grid (level 0) for flow around a square cylinder in 2D

The higher level of computational grids for the numerical studies using dolphin mesh generator presented in the Table 7.5.

Table 7.5: Degrees of freedom for flow around a square cylinder in 2D

Level	Total
0	648
3	37216

Model Parameters

Details of the computational parameters for the test problem flow around a square cylinder are summarized in Table 7.6.

Table 7.6: Computational parameters for flow around a square cylinder

Parameters	Value
Time Iterator	20 :end time
pde:viscosity	4.54545e-5
wall bc	slip-friction slip
solver::equation residual tol	1.0e-6

7.3.1 Comparison of Numerical and Experimental Results

For the time stability, the Courant number, CFL is taken 0.15 in the equation 7.1.

The simulations are performed for the values of the skin friction parameter β where $\beta \in \{0.0001, 0.001, 0.01, 0.1, 0.5, 1.0\}$ and also for the perfect slip and no slip boundary conditions.

The Reynolds number is taken $Re = 2.2e4$ based on the velocity at the inlet and height of the cube, $Re = \frac{\mathrm{uh}}{\nu}$, to compare our results with experimental results. The reattachment length of the recirculating vortex is computed for viscosity parameter $\nu = 4.54545e-5$, given in table 7.6 named as pde:viscosity, and for the grid level 3, 7.5. Computations are presented only for constant inflow profile $u_1 = 1, u_2 = 0$ at the inlet.

The velocity streamlines from the numerical simulations around a square cylinder in two dimension are presented here.

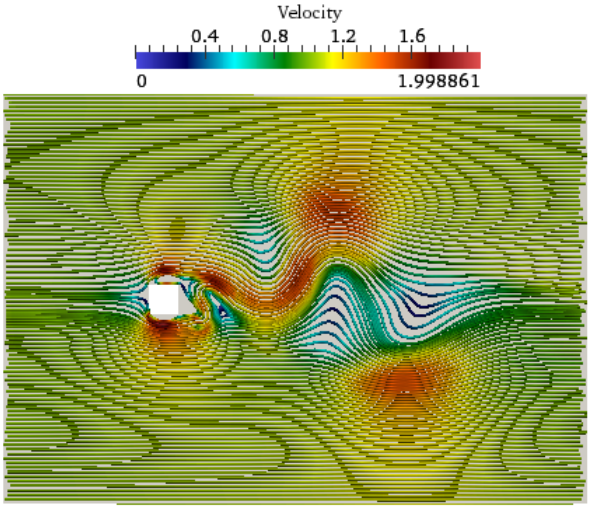

Figure 7.7: Velocity Streamlines for flow around a square cylinder in 2D for $\beta = 0.0$: Numerical Results

The following figures represent the velocity along the centerplane of the square in two dimension. The recovery behind the cylinder of the velocity along the centerplane of the square cylinder is predicted faster and stronger than the experimental results.

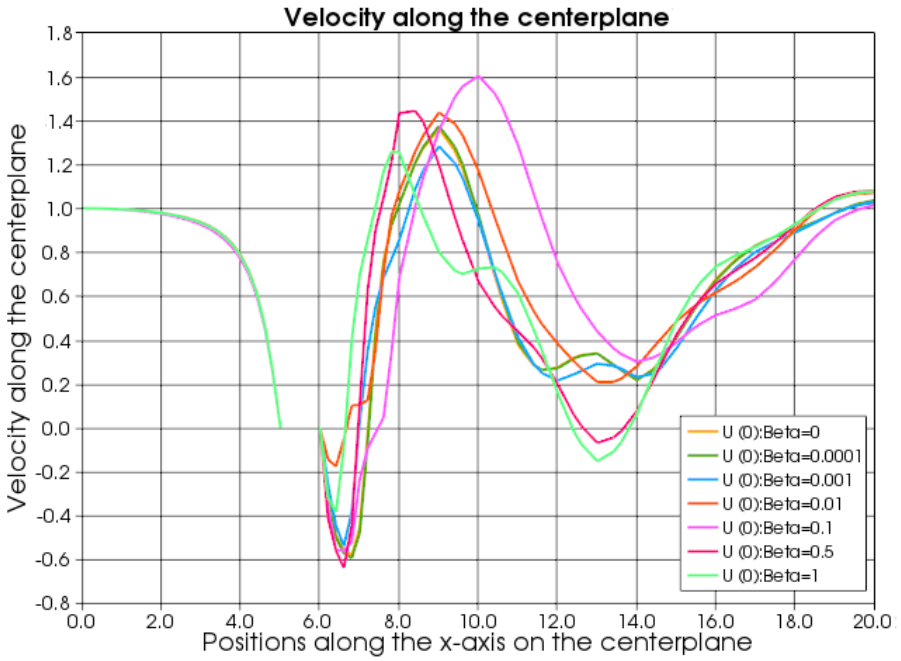

Figure 7.8: Velocity along the centerplane of the square for different values of β

The reattachment lengths defining the length of separation region behind the square cylinder are presented form the experimental and computational works.

Table 7.7: Reattachment length for flow around a square cylinder in 2D (Both Experimental and Computational Results)

Works performed By	Model	Skin-friction (β)	Reattachment Length
Lyn et al. [33]	Experimental	-	1.38
Our Studies	G2 Simulation with Wall Stress Model	$\beta = 0$	1.4
		$\beta = 0.0001$	1.4
		$\beta = 0.001$	1.0
		$\beta = 0.01$	1.0
		$\beta = 0.1$	1.6
		$\beta = 0.5$	1.0
		$\beta = 1.0$	1.0

7.3.2 Remarks

Flow around a square cylinder has quasi-two dimensional character and vortex shedding from the front corner of the square cylinder, so the result of the numerical studies has a much better agreement with the experimental results than the test problem flow around a surface mounted cube.

7.4 Concluding Remarks

We have presented the comparison of numerical results with the available experimental results to validate the wall shear stress model which is a near-wall model that we used in the G2 turbulence simulation technique and we observed a good agreement with the experimental results.

Chapter 8

Observations and Future Works

8.1 Observations

In this project, we have described two different options of near-wall turbulence modeling and their implementation in the G2 turbulence simulation technique. A sensitivity analysis of near-wall turbulence modeling is done by parametric study of model parameters of near-wall turbulence modeling.

We have analyzed the numerical results for the Wall Shear Stress Model as the near-wall turbulence modeling. For the sensitivity analysis of the near-wall modeling we performed the parametric studies of the Wall Shear Stress model and to validate our results we compared our results with the available results from other researchers.

We have also compared our numerical studies with the experimental results available from published works from other researchers to validate the wall shear stress model in G2 turbulence simulation technique.

8.2 Scope of Future Works

We performed the parametric studies of the Wall Shear Stress model with a test problem. There is scope for the future work to perform the simulation with the DDES wall model and then compare the results with the Wall Shear Stress Model.

We have observed that the choice of model parameters depends on the computational mesh, time step. the solution itself and the problem data. Also the choice of skin friction parameter is not certain, so there is scope to work on the uncertainty quantification of the skin friction parameter. And for the uncertainty quantification Monte Carlo approach could be good option where from an ensemble of computed solutions with different parameters, a probability distribution is calculated to predict the resulting distribution of some chosen output from the simulation. Also Sensitivity based methods with Monte Carlo simulation can be performed to analyze the uncertainty quantification.

Bibliography

[1] M. Strelets A. Travin, M. Shur and P. Spalart. Detached eddy simulations past a circular cylinder. *Flow, Turbulence and Combustion*, 63:293–313, 1999.

[2] Klaus-Jurgen Bathe. The inf–sup condition and its evaluation for mixed finite element methods. *Computers and Structures*, 79:243–252, 2001.

[3] Alexander N. Brooks and Thomas J.R. Hughes. Streamline upwind/petrov–galerkin formulations for convection dominated flows with particular emphasis on the incompressible navier–stokes equations. *Computer methods in Applied Mechanics and Engineering*, 32:199–259, 1982.

[4] Uno Navert Claes Johnson and Juhani Pitkaranta. Finite element methods for linear hyperbolic problems. *Computer methods in Applied Mechanics and Engineering*, 45:285–312, 1984.

[5] G. Iaccarino A. Ooi P. A. Durbin and M. Behnia. Reynolds averaged simulation of unsteady separated flow. *International Journal of Heat and Fluid Flow*, 24:147–156, 2003.

[6] A. Ern and J. L. Guermond. *Theory and Practice of Finite Elements*, volume 159. Spriner series: Applied Mathematical Sciences. Springer, 2004.

[7] Peter HANSBO and Anders SZEPESSY. A velocity-pressure streamline diffusion finite element method for the incompressible navier–stokes equations. *Computer methods in Applied Mechanics and Engineering*, 84:175–192, 1990.

[8] Hussein H.J. and Martinuzzi R.J. Energy balance for the turbulent flow around a surface mounted cube placed in a channel. *Phys. Fluids*, 8:764–780, 1996.

[9] Johan Hoffman and Niclas Jansson. A computational study of turbulent flow separation for a circular cylinder using friction boundary conditions. *Quality and Reliability of Large-Eddy Simulations II*, 16:57–68, 2011.

[10] Johan Hoffman and Claes Johnson. *Computational Turbulent Incompressible Flow*. Springer, 2006.

[11] Johan Hoffman and Claes Johnson. A new approach to computational turbulence modeling. *Computational Methods Appl. Mech. Engrg.*, 195:2865–2880, 2006.

[12] Volker John. Slip with friction and penetration with resistance boundary conditionds for the navier-stokes equations-numarical tests and aspects of the implementation. *Journal of Computational and Applied Mathematics*, 147:287–300, 2002.

[13] Rodi W. Ferziger J.H. Breuer M. and Pourquie M. Large eddy simulation: result of a workshop. *J. Fluids Eng.*, 119:248–262, 1997.

[14] Spalart P. Deck S. Shur M. Squires KD. Strelets M. and Travin A. A new version of detached eddy simulation, resistant to ambiguous grid densities. *Theor. Comp. Fluid Dyn.*, 20:181–95, 2006.

[15] Gunzburger MD. *Finite Element Methods for Viscous Incompressible Flows: A Guide to Theory, Practice, and Algorithms.* Academic Press: New York, 1989.

[16] F.R. Menter. Zonal two-equation k-ω turbulence models for aerodynamic flows. *AIAA paper 1993-2906*, 1993.

[17] M. Nazarov. *Adaptive Algorithms and Higher Order Stabilization for Finite Element Computation of Turbulent Compressible Flow.* PhD thesis, Numerical Analysis, NA, KTH, Stockholm, 2011.

[18] Sebastien Deck Pierre Sagaut and Mark Terracol. *Multiscale and multiresolution approaches in turbulence.* Imperial College Press, 2006.

[19] Ugo Piomelli and Elias Balaras. Wall-layer models for large-eddy simulations. *Annu. Rev. Fluid Mech.*, 34:349–374, 2002.

[20] Martinuzzi R. and Tropea C. The flow around surface mounted, prismatic obstacles placed in a fully developed channel flow. *Trans. ASME J. Fluids Eng.*, 115:85–93, 1993.

[21] J. Bodart S. Hickel, E. Touber and J. Larsson. A parametrized non equilibrium wall model for large eddy simulations. In *Proceedings of the Summer Program 2012*, Center for turbulence Research, 2012.

[22] Ramon Codina Santiago Badia and Juan Vicente Gutierrez-Santacreu. Long-term stability estimates and existence of a global attractor in a finite element approximation of the navier–stokes equations with numerical subgrid scale modeling. *SIAM J. NUMER. ANAL.*, 48:1013–1037, 2010.

[23] U. Schumann. Subgrid scale model for finite difference simulations of turbulent flows in plane channels and annuli. *Journal of Computational Physics*, 18:376–404, 1975.

[24] M. Schäfer and S. Turek. Benchmark computations of laminar flow around a cylinder. Technical report, Lehrstuhl fur Strömungsmechanik, Universität Erlangen-Nurnberg, Institute fur Angewandte Mathematik, Universität Heidelberg, Aerodynamisches Institute, RWTH Aachen, Germany, -.

[25] Roger L. Simpson. Turbulent boundary layer separation. *Annu. Rev. Fluid Mech.*, 21:205–34, 1989.

[26] P. R. Spalart. Strategies for turbulence modeling and simulations. *International Journal of Heat and Fluid Flow*, 21:252–263, 2000.

[27] Philippe R. Spalart. Detached-eddy simulation. *Annu. Rev. Fluid Mech.*, 41:181–202, 2009.

[28] M. Strelets. Detached eddy simulation of massively separated flows. *American Institute of Aeronautics and Astronautics, AlAA 2001-0879*, 39, 2001.

[29] S. Taneda. Visualization of separating stokes flows. *J. Phys. Soc. Jpn*, 46:1935–1942, 1979.

[30] A. Scotti U. Piomelli and E. Balaras. *Large-eddy simulation of turbulent flows:from desktop to supercomputer.* In Vecotr and Parallel Processing- VECPAR 2000. J.M.L.M. Palma, J. Donagarra and V. Hernandez, Spriner:Berlin, 2001.

[31] W. Layton V. John and N. Sahin. Derivation and analysis of near wall models for channel and recirculating flows. *An international journal Computers and Mathematics with Applications*, 48:1135–1151, 2004.

[32] S. P. Psychoudaki V. P. Fragos and N. A. Malamataris. Computer aided analysis of flow past a surface mounted obstacle. *International journal for numerical methods in fluids*, 25:495–512, 1997.

[33] Lyn D. A. Einav S. Rodi W. and Park J.H. A laser-doppler velocimetry study of ensemble averaged characteristics of the turbulent near wake of a square cylinder. *J. Fluid Mech.*, 304:205–232, 1995.

Appendix A

Software

A.1 ICORNE:FEniCS-HPC

Software ICORNE, is a rudimentary C++ application framework for FEniCS-HPC, is used to run the simulations. ICORNE implements the General-Galerkin (G2) method and interfaces to other components as such FIAT, FFC and DOLFIN in the FEniCS.

A.1.1 Parametric Launcher:ICORNE

Parametric Launcher is an attractive feature added into the ICORNE farmework that makes the software more generous, more user friendly. To run a simulation using ICORNE, Parametric Launcher includes following features:

1. First, For the input it takes the parameters as a list into the simulation instead of running the simulation separately for each parameter and For each parameter creates different folders with the name of that specific parameter in the output
2. It contains all the solver for the simulation
3. It does the postporcessing of the results at the same time with the output results
4. It ables to do the uncertainty quantification for the results with the various input data; Uses the Monte Carlo Simulation, does the probability distribution of the input and also for the output to give the most accurate prediction of the model parameters

A.2 Mesh Generation

The component DOLFIN-HPC in the framework FEniCS-HPC is used for the mesh genration used into our simulation for the test cases.

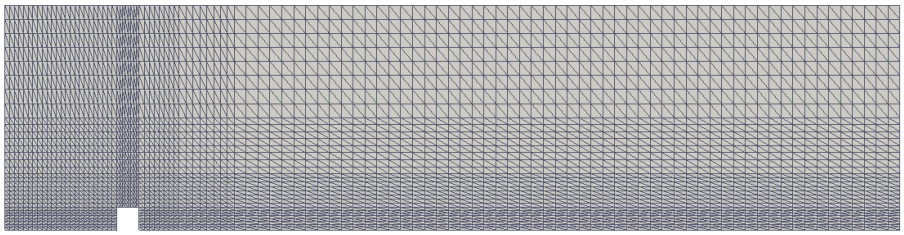

(a) mesh grid : level 3

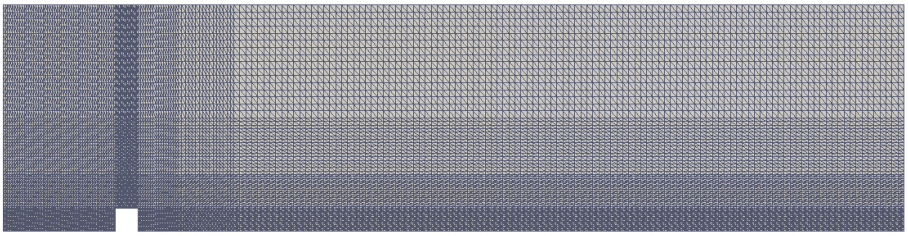

(b) mesh grid : level 4

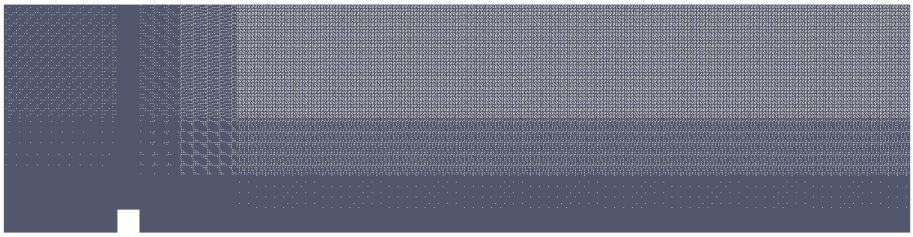

(c) mesh grid : level 5

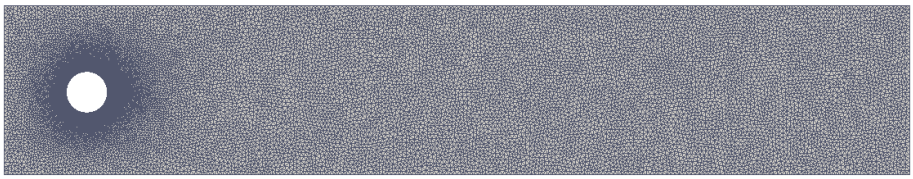

(d) mesh grid : fine and unstructured mesh

Figure A.1: Mesh used into the simulation: step channel and circular cylinder

A.3 Post Processing

For post processing our simulation results, open source software ParaView (Parallel Visualization Application) and GnuPlot are used.

TRITA-MAT-E 2014:33
ISRN-KTH/MAT/E—14/33-SE

www.kth.se